

University of New Mexico

UNM Digital Repository

Civil Engineering ETDs

Engineering ETDs

Spring 5-14-2021

A Practical Methodology to Detect, Quantify and Characterize Experimental Uncertainties in the Dynamic Testing of Structures

James L. Woodall

Follow this and additional works at: https://digitalrepository.unm.edu/ce_etds



Part of the [Acoustics, Dynamics, and Controls Commons](#), and the [Civil Engineering Commons](#)

Recommended Citation

Woodall, James L.. "A Practical Methodology to Detect, Quantify and Characterize Experimental Uncertainties in the Dynamic Testing of Structures." (2021). https://digitalrepository.unm.edu/ce_etds/286

This Thesis is brought to you for free and open access by the Engineering ETDs at UNM Digital Repository. It has been accepted for inclusion in Civil Engineering ETDs by an authorized administrator of UNM Digital Repository. For more information, please contact disc@unm.edu.

James Lee Woodall

Candidate

Civil, Construction, and Environmental Engineering

Department

This thesis is approved, and it is acceptable in quality and form for publication:

Approved by the Thesis Committee:

Fernando Moreu, Chair

John Pott

Tang Tat Ng

**A Practical Methodology to Detect, Quantify and Characterize
Experimental Uncertainties in the Dynamic Testing of Structures**

By

James Lee Woodall

B.S., Civil Engineering,

University of New Mexico, 2018

THESIS

Submitted in Partial Fulfillment of the Requirements for the Degree of

Master of Science,

Civil Engineering

University of New Mexico,

Albuquerque, New Mexico

July 2021

Acknowledgement

I want to thank Dr. Moreu, my advisor and committee chair, as well as Dr. Ng and Dr. Pott for being on my committee. I also want to thank Maimuna Hossain and Odey Yousef for their help in performing this research.

This research has been funded by Sandia National Laboratories. Sandia National Laboratories is a multimission laboratory managed and operated by National Technology & Engineering Solutions of Sandia, LLC, a wholly owned subsidiary of Honeywell International Inc., for the U.S. Department of Energy's National Nuclear Security Administration under contract DE-NA0003525.

This paper describes objective technical results and analysis. Any subjective views or opinions that might be expressed in the paper do not necessarily represent the views of the U.S. Department of Energy or the United States Government.

A Practical Methodology to Detect, Quantify and Characterize Experimental Uncertainties in the Dynamic Testing of Structures

By

James Woodall

B.S., Civil Engineering,

University of New Mexico, 2018

M.S., Civil Engineering,

University of New Mexico, 2021

Abstract

This thesis investigates the uncertainty in the experimental context of structural dynamics. This thesis proposes a method to estimate both the effect of boundary conditions, as well as two different methods to detect the location of sensors on a specimen. Firstly, this thesis proposes a technique to predict the dynamic behavior of any point along a cantilever beam with an uncertain transverse elastic restraint. The technique uses a new conversion expression which relies only on one impact hammer experiment with the whole system, referred to as the complex structure, and a model of the pure cantilever beam, the simple structure. This study validated the proposed method by estimating the Transfer Function (TRF) of the beam and comparing it with an experimentally measured TRF in a system with an uncertain boundary condition using a single input, single output (SISO) test and a model of the simple structure. Secondly, this thesis investigates the estimation of the

location of a sensor given the output data of a physical experiment with two different methods. Researchers often assume sensor location to be precise and reflect this assumption in the creation of Finite Element Models. Small errors in the sensor location may go unnoticed in the frequency domain but can however have an effect in the system identification and generate significant errors in the model accuracy. If these small errors in sensor location could be evaluated and corrected, the experiment could be updated to match the model more accurately. This thesis investigates experimental uncertainties in sensor placement with two separate approaches. One approach investigates the effect of sensor misplacement in the context of modal contributions to find a location error with experimental outputs. The other approach uses a model-matching process similar to a Finite Element Model Update (FEMU) to recognize and estimate a sensor location error. These two methods allow the operator to know if a sensor location should be corrected, and if it should be moved up or down. This thesis demonstrates these approaches by using a steel cantilever beam with two accelerometers, changing the location of one, and implementing the proposed methods to detect the placement error. The two proposed processes can inform researchers of sensor misplacement, either by determining expected error levels based on modal contribution factors, or by matching the eigenvalues of a similar model to those experimentally observed. Researchers can then use this information to correct the deviation in the setup.

Table of Contents

Abstract.....	iv
List of Figures.....	viii
List of Tables	x
Chapter 1: Introduction	1
1.1: Structural Dynamic MIMO Testing	1
1.2: Thesis Outline	1
Chapter 2: Literature Review	4
2.1: Introduction	4
2.2: Uncertain Boundary Conditions.....	4
2.3: Sensor Location Effects	8
Chapter 3: Experiment Specimen and Setup	11
3.1: Specimen	11
3.1.1: Dimensions and Properties	11
3.1.2: Assumptions.....	12
3.2: Equipment	13
3.2.1: Sensors	13
3.2.2: Actuators.....	15
3.2.2: Data Acquisition System	16
3.3: Application.....	17
3.3.1: Finite Element Model	17
3.3.2: MIMO Testing	20
Chapter 4: Transforming a Simple Structure Model to Represent a Complex Dynamic System with Unknown Boundary Restraints	22
4.1: Introduction	22
4.2: Experiment Objective and Research Methodology	22
4.2.1: Complex Structure	22
4.2.2: Dynamic Model of a Simple Structure	24
4.2.3: FE Model Update	28
4.2.4: Research Methodology	29
4.3: Transformation Derivation	30

4.3.1: Boundary Condition	30
4.3.2: Application	32
4.4: Experiment and Results	34
4.4.1: SISO Experiment	34
4.4.2: Complex Structure Measured TRF	35
4.4.3: Complex Structure TRF Estimation	35
4.4.4: Results and Analysis	36
4.5: Conclusions	41
Chapter 5: New Methodologies to Identify and Correct the Mislacements of Sensor Location in Experimental Dynamics	43
5.1: Introduction	43
5.2: Methodology	43
5.2.1: Modal Contributions Method.....	44
5.2.2: Model-matching Method	47
5.3: Experiment	48
5.3.1: Physical Setup.....	48
5.3.2: Experiment Process	49
5.3.3: Sensor Location Error Effects.....	51
5.4: FEM.....	53
5.5: Results	54
5.5.1: Modal Contributions Results	54
5.5.2: Model-matching Results	61
5.6: Conclusions	63
Chapter 6: Conclusions	64
6.1: Summary	64
6.1.1: Uncertain Boundary Conditions	64
6.1.2: Sensor Location Effects	65
6.2: Future Work	66
References	68
Appendix.....	74

List of Figures

Fig. 2-1: Modal Analysis Test Vehicle Setup after Test Design with a Model	5
Fig. 2-2: Compound Substructures	6
Fig. 3-1: Base Beam Diagram.....	12
Fig. 3-2: PCB Accelerometer.....	14
Fig. 3-3: PCB Force Transducer	14
Fig. 3-4: Impact Hammer.....	15
Fig. 3-5: Smartshaker.....	16
Fig. 3-6: Vibpilot	17
Fig. 3-7: 2 DOF Beam Example	18
Fig. 3-8: MIMO Test Setup	21
Fig. 4-1: Complex Structure Setup	23
Fig. 4-2: BC Attachment Effects on Example TRF.....	24
Fig. 4-3: FEM Representation.....	25
Fig. 4-4: Simple Case Mode Shapes	27
Fig. 4-5: Model Vs. Experimentally Measured TRFs at 1/3 Height	29
Fig. 4-6: Combining the FEM of a Simple Structure with a SISO Experiment.....	30
Fig. 4-7: TRF H_{Sting} Description	32
Fig. 4-8: Experiment with Complex Structure	35
Fig. 4-9: Estimated vs. Experimentally Measured TRFs at the Tip	37
Fig. 4-10: Complex Case Measured and Estimated Mode Shapes	39
Fig. 5-1: Two Methods for Detecting Sensor Placement Error	44
Fig. 5-2: Modal Contribution Application	45
Fig. 5-3: Modal Contributions	46
Fig. 5-4: Experiment Setup	49
Fig. 5-5: Experiment TRFs	50
Fig. 5-6: Sensor Location Effect Test	51
Fig. 5-7: Sensor Location Effect Time Histories	52
Fig. 5-8: Sensor Location Effect Summary	53

Fig. 5-9: FEM Representation	54
Fig. 5-10: Broadband Input Time Signals.....	55
Fig. 5-11: Broadband Input Results: Simulation and Experiment.....	56
Fig. 5-12: Broadband Input Results: Different Intervals	58
Fig. 5-13: Broadband Input Frequency Domain	59
Fig. 5-14: % Contribution to Response.....	60
Fig. A-1: Experiment MC Sum vs. GRMS	75
Fig. A-2: Simulation MC Sum vs. GRMS	75

List of Tables

Table 3-1: Natural Frequency Comparison.....	19
Table 3-2: Modal Damping Comparison	19
Table 4-1: Natural Frequency Comparison.....	26
Table 4-2: Modal Damping Comparison	26
Table 4-3: Comparison of Estimated and Measured TRFs Frequency Ranges	37
Table 4-4: Comparison of Estimated and Measured TRF Natural Frequencies	38
Table 5-1: Sensor Placement Error	50
Table 5-2: Mode Frequencies	50
Table 5-3: Model Location Metric Scores and Sensitivities.....	51
Table 5-3: Model Location Metric Scores and Sensitivities.....	51
Table A-1: Linear Regression Slopes	76

Chapter 1: Introduction

1.1: Structural Dynamic MIMO testing

Researchers use Multiple-Input, Multiple Output (MIMO) in structural dynamic testing for many fields. These range from building earthquake engineering to component testing for machinery such as in air and spacecraft. In the often-complex realm of dynamics, MIMO offers a variety of tools for understanding and effectively replicating field environments within the laboratory. This allows researchers to efficiently evaluate theories, designs, and components by testing them within the lab in a controlled environment, rather than in the field at full scale. Additionally, researchers use MIMO in the lab to check model legitimacy and perform model updates.

Despite MIMO's prevalence in structural dynamic testing, researchers still have much to learn. The plethora of journal papers being published about different aspects of MIMO testify both its widespread application and the fact that it is still a field under development, with many issues to improve and resolve. There are many aspects of MIMO that researchers are working to understand, such as boundary conditions, signal processing, nonlinearities, as well as many others. This thesis focuses on certain issues dealing with uncertain boundary conditions, and uncertainty in effects of sensor placement location.

1.2: Thesis Outline

This thesis investigates sources of uncertainty in MIMO dynamic structural testing, using a steel cantilever beam as the example specimen. This study performs experiments on SIMO systems for simplicity and to better control the test environment,

but the topics examined can extrapolate to apply to MIMO. Below is a summary of each subsequent chapter in this thesis.

Chapter 2 investigates the current state of literature with respect to the topics presented in this thesis, describing the relative strengths and weaknesses they demonstrate. This chapter also touches on how the research in this thesis augments and builds on the current state of knowledge within structural dynamic MIMO testing.

Chapter 3 provides an in-depth description of the specimen and the equipment relevant to this thesis. Specimen dimensions and properties are discussed, as well as the assumptions underlying its application in this work. This chapter also summarizes the sensors, DAQs, and actuators that this research implemented in testing. Finally, Chapter 3 briefly reviews some related work that builds on and supports the research in this thesis.

Chapter 4 presents the research pertaining to uncertainties in boundary conditions, reporting the experimental technique this thesis proposes for transforming a model to represent a more complicated system. This chapter also evaluates the performance of this technique at a range of frequencies, as found in an example experiment, and describes the overall strengths and weaknesses it possesses relative to the current standard approach.

Chapter 5 discusses the research involving the use two techniques to identify the precise location of sensors in a physical test, given the output responses of an experiment. The first of these techniques incorporates the use of modal contributions with respect to the input signal to justify and explain patterns in error. The second technique uses a model-matching technique to identify sensor placement error by

selecting a model with sensor locations such that the natural frequencies match as closely as possible. In this chapter, there are different metrics for performing this model update, which the study analyzes and compares against each other, as well as indicating where there is a need for further research.

Chapter 6 summarizes the results from Chapters 4 and 5, as relevant within the context presented in this chapter and Chapter 2. Chapter 6 discusses the conclusions of the work presented in this thesis, as well as the future work left going forward to further enhance the field and improve the capabilities of those who work in it.

Chapter 2: Literature Review

2.1: Introduction

This chapter presents an overview of the methods, techniques, and investigations offered by researchers concerning the topics discussed in this thesis. This chapter discusses the shortcomings of the available resources and how the current state of knowledge warrants the research this study encompasses. First, the literature review delves into the problem of Uncertain Boundary Conditions. Second, it discusses the problem of Sensor Location Effects, with an emphasis on uncertainty in sensor locations and the resultant error in a system's mass matrix.

2.2: Uncertain Boundary Conditions

Researchers use models to design experiments prior to their implementation to help to establish input design as well as sensor and input locations [1-5], as Figure 2-1 illustrates. However, differences between generated models and real-world systems often cause misrepresentation of the system, which results in errors. Consequently, researchers must take uncertainties into account when using models to design an experiment [6]. Even though models are valuable to design tests, sometimes there is not enough information available to inform these models.

Boundary conditions are an important part of models, but are often difficult to represent accurately, especially if its dynamic properties are unknown. Researchers use models to design experiments to test structures for vibration, shock, and impact analysis [7], but analytical models must properly represent the structure to be effective [8-9]. These boundary conditions complicate the structure, and the model must include their effects to represent it properly [10]. However, for dynamic analysis, theoretical models do not always

accurately consider the physical boundary conditions [11]. The model of a simple structure that does not represent the dynamic effects of any supports or attachments on it will result in errors if a researcher uses it inappropriately.



Fig. 2-1: Modal Analysis Test Vehicle Setup after Test Design with a Model [4]

The properties of the restraints in structural models are not always available. Modeling elastic restraints such as stingers on a beam typically requires understanding their

dynamic properties [12-13]. Specifically, researchers have developed methods to create a modal model for both the complex, coupled structure, and its independent components [14]. Figure 2-2 illustrates this substructuring process. However, they assume sufficient knowledge concerning the nature of the boundary conditions, which is not always available. While researchers have investigated methods to model uncertainties in these parameters [15-16], the quality of a model ultimately depends on the quality of the parameters assumed.

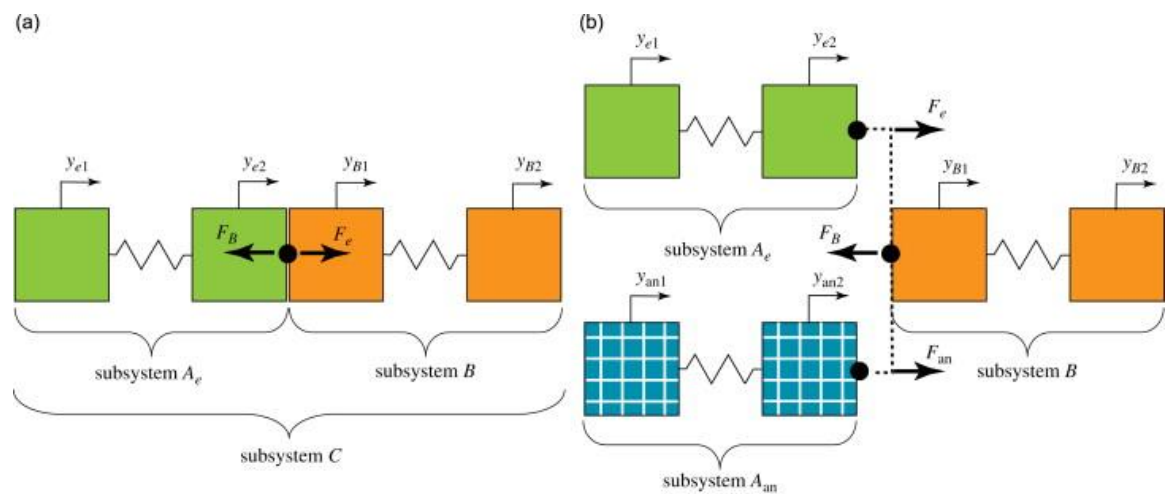


Fig. 2-2: Compound Structures [14]

Substructuring uses either an analytical model such as an FE model or a modal model that consists of measured TRFs. Each of these has inherent strengths and weaknesses [17]. A FE model requires a high degree of computational power and storage, in addition to being difficult to accurately represent the setup [18]. Researchers have investigated methods to reduce and simplify models to be more computationally accessible while maintaining a reasonable degree of accuracy, but the problem is still unsolved [19-21]. Likewise, using an experiment based modal model requires sensors to measure the outputs at every relevant location. The number of sensors can be limited, and adding sensors

changes the dynamic properties, often requiring an analytical model to remove their effects [22-24].

Structural Dynamic Modification (SDM) theory [25-26] has a similar approach for identifying changes in a structure [25]. While the theory involves both applying measured TRFs and analytical models [26], researchers tend to use it for “black box systems,” where the system is too complex for a purely analytical model to be practical [27]. SDM has many of the same strengths and weaknesses as substructuring, allowing for accurate, well-informed results, at the expense of large, difficult models or intensive experimental analysis. Some analogies to SDM can be found in this method including, but not limited to, Sestiere [29]. Their work covers equations explaining the generalized effect of a system alteration to the dynamic properties given the change in mass, stiffness, and damping which the alteration causes. This study discusses a novel approach to a 1DOF imposed restraint case on a cantilever beam that can be applied using the results obtained from a single sensor and test, without knowledge of how exactly the fundamental matrices describing the system change. Additionally, this thesis discusses its application in the laboratory and obtaining these transfer functions as the source of information for the mathematical derivation. This study presents a simplified experimental technique as a laboratory adoption of the simplified mathematical model. This implementation enables the estimation of the changes in a laboratory specimen after one degree of complexity is added. The method presented in this thesis provides a way to make similar estimations with less involved steps required. In summary, substructuring and SDM are useful tools, with their own limitations as well.

Chapter 4 of this thesis provides and tests a novel method that combines the model of a simple structure and the result of a SISO experiment with the complex structure to

estimate the TRFs of output locations not found in the test. A cantilever beam with a stinger attached as a partial transverse restraint comprises the complex structure. The proposed method requires less foreknowledge than building a Finite Element Model for the entire system and is easier to implement than directly measuring the TRFs for every possible output, as necessitated by many of the current practices.

2.3: Sensor Location Effects

Experiments play a major role in structural dynamic research such as modal analysis. Researchers use experiments to learn about the natural world, validate theories, and test components. These experimental applications help improve safety in different industries and advance the state-of-the-art knowledge in the field. As a result, it is important for researchers to have a high degree of confidence that the experiment they perform is the experiment they think they are performing. Deviations between the intended experiment and what is performed can result in large errors that may completely change the conclusion of a test if not caught and properly addressed [6]. These deviations between intended and performed experiments can occur across many different aspects of a test, and the effects can range from being negligible to highly consequential. This forces the researcher to understand the sensitivity of these parameters with respect to the dynamic response of the system as well as the uncertainty associated with each one [30-32]. These parameters cover aspects of the experiment from input loads to boundary conditions to sensor placement, which is the subject of Chapter 5.

The presence of sensors on a Subject Under Test (SUT) can cause discrepancies between reality and the researcher's idea of what they are testing. When these discrepancies are too severe, researchers must find ways to reconcile the systems [33]. One method of

doing this is by mitigating the effect of the sensor on the real system [34-37]. Researchers also reconcile the systems by including the mass of the sensor within a model to match their presence in an experiment. Once the model adequately matches the experiment, the sensor masses may be removed from the model to better simulate the behavior of the SUT in the field, when no sensors are present. However, many of these methods assume the location of the sensors to be known precisely, and the decoupling procedures can be prone to severe error propagation [38]. The dynamic effect of sensor mass cannot be ignored in many tests, such as those in which the sensor mass is not insignificant compared to that of the SUT.

Chapter 5 of this thesis investigates the estimation of the location of a sensor given the output data of a physical experiment. One way the research does this by demonstrating the effect of a small misplacement of the sensor on the system outputs and performing a process similar to a model update by iteratively changing the positions of the sensors. Several methods of performing a Finite Element Model Update (FEMU) indirectly move the mass of the sensors in a model by updating the Mass Matrix [39]. When sensor mass is significant relative to the nodal mass of the FEM, then focusing specifically on sensor location will yield similar results as reevaluating the entire mass matrix. Comparing output results from a real experiment with those from a model can only be done effectively if the sensor or output locations are truly analogous. This chapter demonstrates the ability of a model update to detect the misplacement of the sensor and allow the researcher to correct the error. It achieves this by creating a Finite Element Model (FEM) of the cantilever beam using the same geometric and material properties as the experimental beam and altering it with the iterative movement of a sensor location in the model until the model natural

frequencies best match those of the test. Another way this chapter investigates the estimation of the location of a sensor given the output data of a physical experiments by the application of insights offered by modal contributions to identify errors in sensor location. This chapter demonstrates this by finding the modal contributions of each mode at a range of frequencies and combining this with the input signal frequency magnitudes to indicate the extent to which each mode is relevant for a given input signal. The thesis examines the variation in each mode per a change in sensor location considering this parameter to justify and explain the patterns of error in the experiment. These methods potentially allow for the correction of placement errors in a physical experiment, as well as a deeper understanding of how the errors affect the dynamic response of the system.

In summary, the work presented in this chapter demonstrates the ability of these two methods to detect the misplacement of a sensor. Since the methods rely on detecting changes in the dynamic properties, they will be most effective in experiments where the mass of the sensors relative to the mass and stiffness of the structure are not insignificant, while offering little insight for large, very stiff structures with small, light sensors. These techniques potentially allow for the correction of sensor placement errors in a physical experiment.

Chapter 3: Experiment Specimen and Setup

This chapter details the specimen, the equipment, and the base setup this thesis uses. Subsequent chapters will reiterate some of these details, as relevant to each experiment, as well as describing what factors distinguish them from other tests or the base setup. This chapter also gives a brief introduction to other research performed with similar setups, and how they either build on or lead to the work presented in this thesis.

3.1: Specimen

3.1.1: Dimensions and Properties

This thesis examines a base structure of a hot rolled steel cantilever beam. The beam is 1.5 inches wide, by 1/8th of an inch thick (3.81x0.3175 cm). This thesis uses 2 beams with this cross-section in the experiments and models. Chapter 4, which discusses uncertain boundary conditions, uses a 33 inch-long beam (83.82 cm), while Chapter 5, which discusses sensor location, uses a 34.5 inch-long beam (87.63 cm). Two sensors attach to the beam for the work presented in this thesis, one attaches at the tip, and one attaches at the one third point. Each of these sensors connects to the beam via a magnetic plate. The combined mass of each sensor with its respective plate is 0.0952 lb-mass, or 43.2 grams.

The base of the beam is tightly clamped between two ½ inch (1.27 cm) thick steel plates, which are in turn tightly clamped to a 1.5 inch by 3 inch (3.81x7.62 cm) stretch of 80/20 aluminum framing, which bolts into the concrete strongwall and foundation. The experiments have arranged the setup such that all forces applied to the beam act to excite the beam about its flexible axis and are aligned with the framing member's strong axis. Figure 3-1 illustrates the base beam setup.

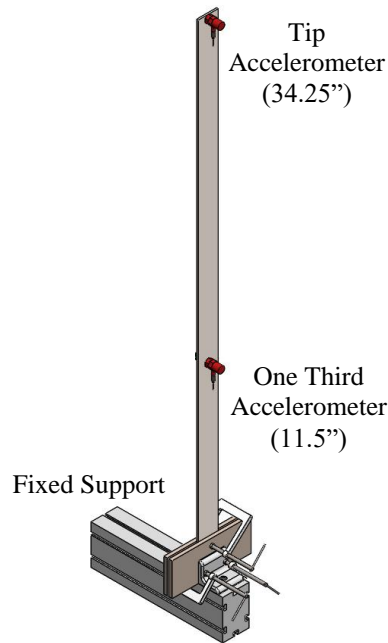


Fig. 3-1: Base Beam Diagram

3.1.2: Assumptions

The work in this thesis makes several notable assumptions concerning the nature of the physical setup. Many of the effects of these assumptions are most likely negligible, but it is nonetheless important to recognize what they are and to what extent they may or may not be valid.

The first primary assumption is that of fixity. This study assumes that the base of the cantilever beam is perfectly rigid. In the real world, this assumption can never be true, but this research considers the effects of any non-rigidity to be negligible within the scope of the work presented. This thesis provides no work or conclusions for frequencies higher than 200 Hz, while the effects of fixity in these types of settings tends to affect higher orders of magnitude frequencies.

The next main assumption is that of linearity. Like fixity, true linearity does not exist in the real world, but this study treats the beam and all related dynamic systems as

though they are perfectly linear. The work presented in this thesis relies on small-scale forces and deflections, where the maximum displacements along the beam are well below 5% of the beam's length. As a result, the work in this thesis treats suspected sources of non-linearity such as the sensor cords and air resistance as negligible.

Each test also assumes that all forces which the beam experiences are perpendicular to the plane of the broad side of the beam. Different tests actuate the beam either with an impact hammer or a stinger-based actuator, with those using the actuator as the more liable to violate this assumption. This is due to the potential change in angle where the stinger connects to the beam as the beam vibrates, causing the stinger to impose a small moment as it deflects to accommodate the vibration. Since the deflections of the beam were kept small, this research considers any rotational or lateral forces applied by the stinger to be negligible.

3.2: Equipment

3.2.1: Sensors

The experiments in this thesis use two piezoelectric accelerometers to observe and record experiment outputs. These sensors are Model 353B03 accelerometers, from PCB Piezotronics. They have a measurement range of $\pm 500g$, with a broadband resolution of 0.003 g. Using a quartz-shear sensing element, it can accurately measure frequencies between 1 and 7000 Hz. Figure 3-2 illustrates one of these sensors, with PCB Piezotronics' website providing the picture [40].



Fig. 3-2: PCB Accelerometer [40]

When a stinger excites the beam, load cells are placed between the stinger and the beam to collect and record the applied input forces. These load cells are Model 208C02 Force Sensors. Like the accelerometers, PCB Piezotronics produces these sensors, and provided the picture on their website [41]. These sensors can accurately measure up to 100 lbf, at a frequency range of 0.001 to 36,000 Hz, with a broadband resolution of 0.001 lbf. Figure 3-3 provides a picture of one of these sensors.



Fig. 3-3: PCB Force Transducer [41]

3.2.2: Actuators

The experiments in this thesis use two methods for exciting the structure. The first of these is with an impact hammer. This piece of equipment is a Model 086C03 modally tuned impulse hammer. Manufactured by PCB Piezotronics, it can measure up to 500lbf of force with its quartz sensing element. The hammer has a total length of 8.5 inches (21.59 cm), with a tip diameter of 1/4th of an inch (0.635 cm). The resonant frequency of the hammer is well beyond the range relevant to the scope of these tests at over 22,000 Hz.



Fig. 3-4: Impact Hammer

In addition to an impact hammer, experiments incorporate the application of an electrodynamic magnet shaker, which excites the structure via nylon 10-32 stingers, which connect to the beam with magnetic plates. The actuators used are Model K2007E01 Smartshakers, manufactured by The Modal Shop Inc., with up to 7 lbf peak sine force and maximum shock force of 15 lbf. This shaker has a double amplitude maximum stroke length of 1/2 of an inch, and has a peak acceleration of 70 g when unloaded, or 3.3 g when loaded at maximum capacity with 2 lb. This shaker is illustrated in Figure 3-5.

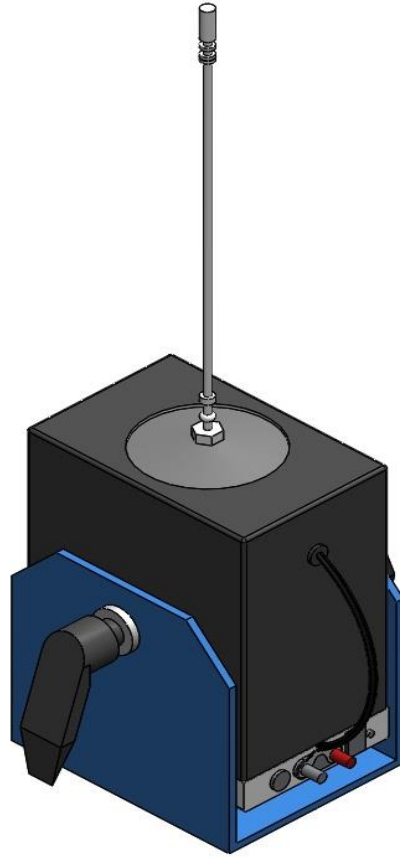


Fig. 3-5: Smartshaker

3.2.3: Data Acquisition System

Experiments used an 8-channel Data Acquisition system (DAQ) to collect and record the signals generated by the sensors. The DAQ is the VibPilot, which m+p international produces. This DAQ receives data with 24-bit analog-to-digital converters (ADCs) up to a 102.4-kHz antialiased sampling rate. This hardware also has 2 source output channels, which input the relevant signals to the Smartshaker when it excites the beam. Figure 3.6 depicts this DAQ, m+p providing the picture [42].



Fig. 3-6: VibPilot [42]

3.3: Application

3.3.1: Finite Element Model

This thesis frequently uses a Finite Element Model to represent the structures examined. As well as being an integral part of some of the methods proposed in this thesis, this tool allows for virtual simulations to be performed. Virtual simulations have several advantages to help augment physical experiments. These include the ability to isolate sources of error, predict the results of changes to the physical setup, and better investigate some of the underlying theory to better understand the way the physical setup behaves.

This thesis uses an FEM of the beam which is a Euler-Bernoulli beam. After creating the Mass and Stiffness matrices with a MATLAB[®] code the eigenvectors and eigenvalues were calculated. Sensors are represented by lump masses applied to the Mass matrix as appropriate depending on their location. Using the Log-decrement method on an experiment allowed a damping estimate, which was used with the Mass and Stiffness Matrices to create a state-space model within MATLAB[®]. The research uses this state space model to take the virtual system and perform different simulations and modal analyses. Each time the research used this FEM, the code implementing it started from the

definitions of these parameters. This allows changes in properties such as height or sensor location to be easily addressed and altered to best match the experimental case.

As an example for how this thesis derives and applies this model, consider a simple 2 DOF cantilever beam with no damping.

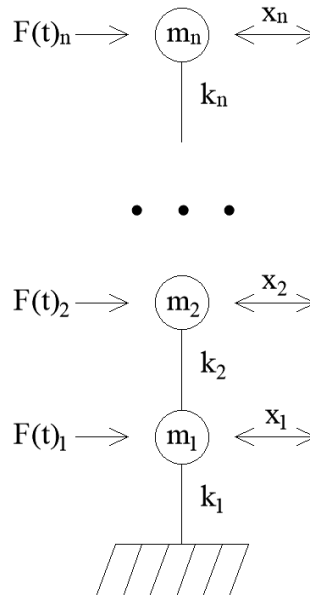


Fig. 3-7: 2 DOF Beam Example

Based on Newtons Equations of motion:

$$m_i \ddot{x}_i = F(t)_i + x_i k_i - (x_i - x_{i+1}) k_2 \quad (3.1)$$

, where m_i is the mass of node i , \ddot{x}_i is the acceleration at node i , $F(t)_i$ is the external force applied at node i , x_i is the displacement at node i , and k_i is the stiffness of the element associated with node i . Defining the parameters as vectors and matrices,

where n is the number of nodes:

$$p(t) = \begin{bmatrix} F(t)_1 \\ F(t)_2 \\ \dots \\ F(t)_n \end{bmatrix}, K = \begin{bmatrix} k_1 + k_2 & -k_2 & 0 & 0 \\ -k_2 & k_2 + k_3 & \dots & 0 \\ 0 & \dots & \dots & \dots \\ 0 & 0 & \dots & k_n \end{bmatrix}, M = \begin{bmatrix} m_1 & 0 & 0 & 0 \\ 0 & m_2 & 0 & 0 \\ 0 & 0 & \dots & 0 \\ 0 & 0 & 0 & m_n \end{bmatrix} \quad (3.2)$$

Therefore, rearranging into matrix form:

$$\begin{bmatrix} m_1 & 0 & 0 & 0 \\ 0 & m_2 & 0 & 0 \\ 0 & 0 & \dots & 0 \\ 0 & 0 & 0 & m_n \end{bmatrix} \begin{bmatrix} \ddot{x}_1 \\ \ddot{x}_2 \\ \dots \\ \ddot{x}_n \end{bmatrix} = \begin{bmatrix} k_1 + k_2 & -k_2 & 0 & 0 \\ -k_2 & k_2 + k_3 & \dots & 0 \\ 0 & \dots & \dots & \dots \\ 0 & 0 & \dots & k_n \end{bmatrix} \begin{bmatrix} x_1 \\ x_2 \\ \dots \\ x_n \end{bmatrix} + \begin{bmatrix} F(t)_1 \\ F(t)_2 \\ \dots \\ F(t)_n \end{bmatrix} \quad (3.3)$$

Define state vectors $q(t)$ and $\dot{q}(t)$ as vectors of the beam response as given by the equations:

$$q(t) = \begin{bmatrix} x_1 \\ x_2 \\ \dots \\ x_n \\ \dot{x}_1 \\ \dot{x}_2 \\ \dots \\ \dot{x}_n \end{bmatrix} \quad \therefore \quad \dot{q}(t) = \begin{bmatrix} \dot{x}_1 \\ \dot{x}_2 \\ \dots \\ \dot{x}_n \\ \ddot{x}_1 \\ \ddot{x}_2 \\ \dots \\ \ddot{x}_n \end{bmatrix} \quad (3.4)$$

Define State Space Matrices State Matrix A and Input Matrix B such that

$$[\dot{q}(t)] = [A][q(t)] + [B][p(t)] \quad (3.5)$$

$$A = \begin{bmatrix} [0] & [I] \\ [-K \times inv(M)] & [0] \end{bmatrix}, \quad B = \begin{bmatrix} [0] \\ [inv(M)] \end{bmatrix} \quad (3.6)$$

, where [0] is a nxn matrix of zeros, and [I] is a nxn identity matrix. Combining into the State Equation:

$$\begin{bmatrix} \dot{x}_1 \\ \dot{x}_2 \\ \dots \\ \dot{x}_n \\ \ddot{x}_1 \\ \ddot{x}_2 \\ \dots \\ \ddot{x}_n \end{bmatrix} = \begin{bmatrix} [0] & [I] \\ [-K \times inv(M)] & [0] \end{bmatrix} \begin{bmatrix} x_1 \\ x_2 \\ \dots \\ x_n \\ \dot{x}_1 \\ \dot{x}_2 \\ \dots \\ \dot{x}_n \end{bmatrix} + \begin{bmatrix} [0] \\ [inv(M)] \end{bmatrix} \begin{bmatrix} F(t)_1 \\ F(t)_2 \\ \dots \\ F(t)_n \end{bmatrix} \quad (3.7)$$

The vector Y represents the total output, as found by multiplying $q(t)$ by the output matrix C and $p(t)$ by the feedthrough matrix, D. Since this example examines the

outputs of all nodes, the output equation effectively just builds on the state space equation.

$$Y = \begin{bmatrix} x_1 \\ x_2 \\ \dots \\ x_n \\ \dot{x}_1 \\ \dot{x}_2 \\ \dots \\ \dot{x}_n \\ \ddot{x}_1 \\ \ddot{x}_2 \\ \dots \\ \ddot{x}_n \end{bmatrix}, \quad C = \begin{bmatrix} [I] & [0] \\ [0] & [I] \\ [-K \times \text{inv}(M)] & [0] \end{bmatrix}, \quad D = \begin{bmatrix} [0] \\ [0] \\ [\text{inv}(M)] \end{bmatrix} \quad (3.8)$$

$$[Y] = [C][q(t)] + [D][p(t)] \quad (3.9)$$

Substituting into Equation 9:

$$\begin{bmatrix} x_1 \\ x_2 \\ \dots \\ x_n \\ \dot{x}_1 \\ \dot{x}_2 \\ \dots \\ \dot{x}_n \\ \ddot{x}_1 \\ \ddot{x}_2 \\ \dots \\ \ddot{x}_n \end{bmatrix} = \begin{bmatrix} [I] & [0] \\ [0] & [I] \\ [-K \times \text{inv}(M)] & [0] \end{bmatrix} \begin{bmatrix} x_1 \\ x_2 \\ \dots \\ x_n \\ \dot{x}_1 \\ \dot{x}_2 \\ \dots \\ \dot{x}_n \end{bmatrix} + \begin{bmatrix} [0] \\ [0] \\ [\text{inv}(M)] \end{bmatrix} \begin{bmatrix} F(t)_1 \\ F(t)_2 \\ \dots \\ F(t)_n \end{bmatrix} \quad (3.10)$$

This illustrates the fundamental method used to generate the FE models in this research. The models this research incorporates are complicated only by the application of damping, the consideration of rotational DOFs, and simply using more than two nodes.

3.3.2: MIMO Testing

Besides the results discussed in this thesis, there is other related work which uses a similar beam to perform research in MIMO testing. The results in this thesis are only single input, as the research investigates the individual sources of uncertainty in MIMO on a smaller

scale, but some testing involves true MIMO experiments. For one of these, a series of simple Multiple Input Multiple Output (MIMO) tests were performed on a cantilever beam to establish a measure of test-to-test variation and investigate how this reflected in the relevant TRFs and inputs which were estimated with inverse MIMO. These tests used two input stingers. Figure 3-8 depicts the physical setup for these tests.

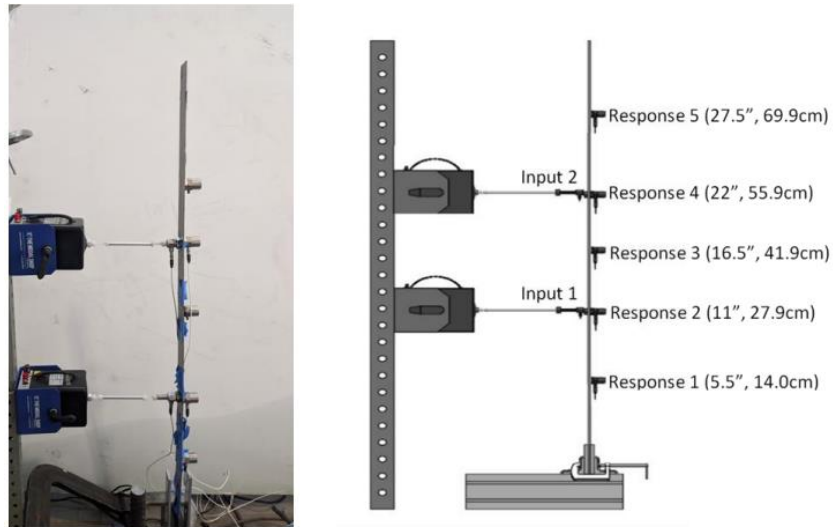


Fig. 3-8: MIMO Test Setup

The series of experiments consisted of a three-test process, which was performed four times. The first of these tests actuated the beam with Input 1, while Input 2 received no signal. The second test actuated the beam with Input 2, while Input 1 received no signal. The research calculated independent TRFs from each input location from these two tests. Finally, both Inputs actuated the beam simultaneously.

This experiment provides many aspects of MIMO to analyze, such as shaker interaction, stinger stiffness effects, and noise variability. Using the research presented in this thesis will allow for even deeper investigation, potentially eventually removing the effects of non-axial loads from the stingers and ensuring adequate sensor placement on the beam.

Chapter 4: Transforming a Simple Structure Model to Represent a Complex Dynamic System with Unknown Boundary Restraints

4.1: Introduction

This chapter provides and tests a novel method that estimates the TRFs of a complex structure. This method combines the model of a simple structure and a SISO experiment with the complex structure to make these estimations. This study compares an experimentally measured TRF with one estimated with this method for validation. This method requires less foreknowledge than building a Finite Element Model for the entire system and is easier to implement than directly measuring the TRFs for every possible output.

4.2: Experiment Objective and Research Methodology

This chapter experimentally estimates the dynamic properties of a complex structure with knowledge of the simple system, only one SISO experiment, and no information of the complex boundary condition. The following sections describe the complex structure selected for this experiment, the simple system model, and the research methodology.

4.2.1: Complex Structure

A 33 inch (83.82 cm) long steel cantilever beam which clamped to a stiff frame is the specimen for these tests. Sensors measuring the output acceleration attached at the tip and the 1/3rd mark respectively. A stinger, representing a partial transverse restraint, connected at the 1/3rd location as well. This component rigidly attached to a strong wall and constituted the uncertain boundary condition/component attached to the simple structure, turning it into a complex structure. This attachment changed the dynamic properties of the

system significantly, rendering a model of the simple structure obsolete by itself. Figure 4-1 displays this setup.

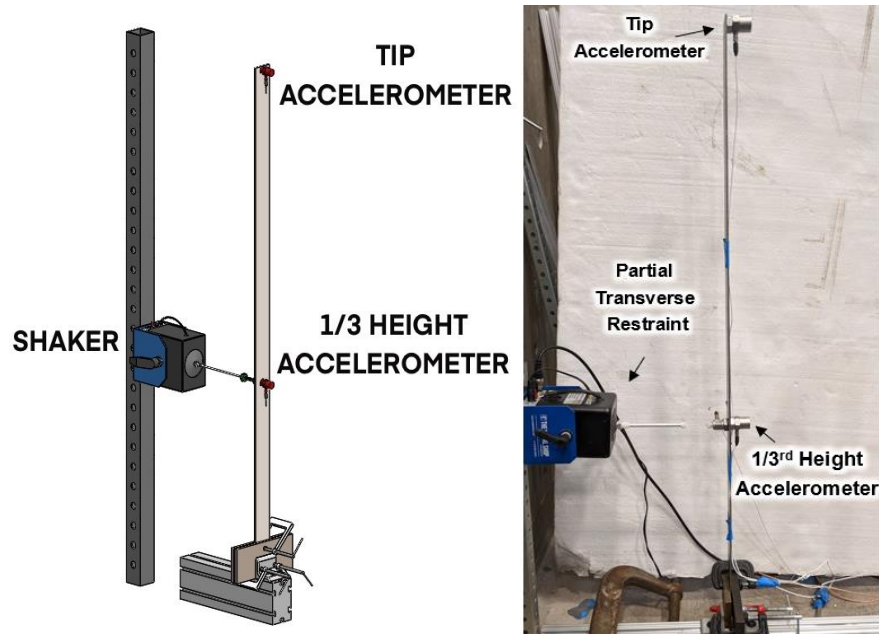


Fig. 4-1: Complex Structure Setup

This thesis refers to the new structure as the “complex structure” which includes the new complex dynamic system composed of just a single structure with the complex attachments. This nomenclature for the manuscript allows the comparison of two analogous structures: simple structure (without complex boundary conditions) and complex structure (simple structure with complex attachments). Additionally, this generalizes the process to be more versatile.

Figure 4-2 depicts the TRF relating the acceleration response at the tip of the beam to the force input applied by the impact hammer at one third its height, before and after applying the uncertain boundary condition. This demonstrates the changes in mode for transforming the simple structure to a complex, illustrating the well-documented problem

this study tries to address. Within the frequency range observed, the attachment of the boundary condition squeezes the modal frequencies to shift in towards 30 Hz. This is most evident in the second, third, and fifth modes. These modes also increase in damping significantly when the system is changed to a complex structure.

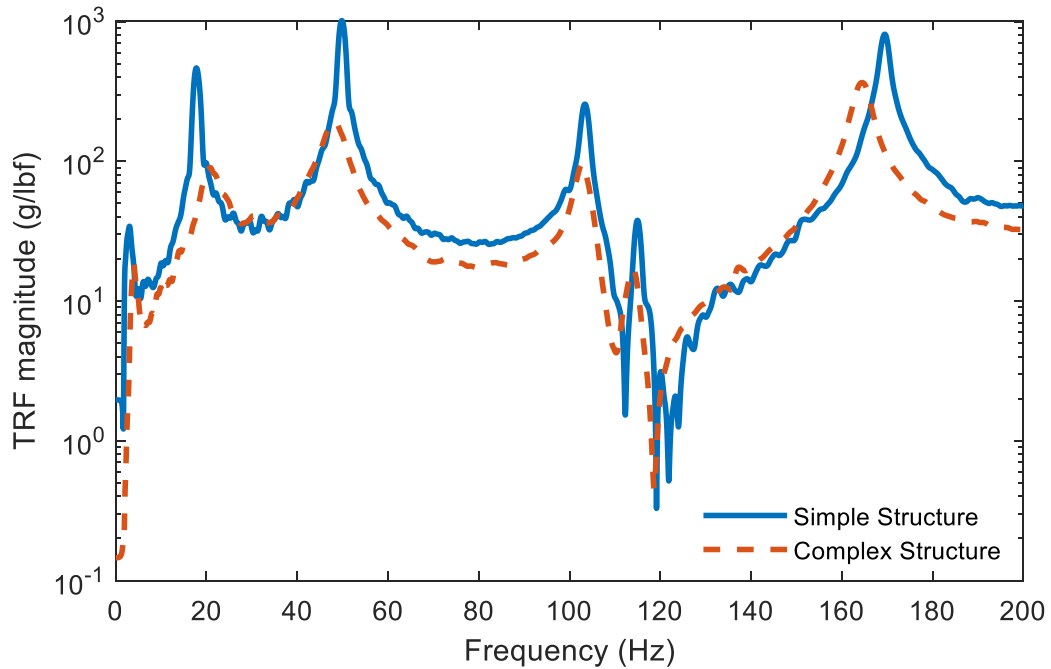


Fig. 4-2: BC Attachment Effects on Example TRF

4.2.2: Dynamic Model of Simple System

A Finite Element (FE) model of the simple structure without a stinger attached uses the same geometric and material properties as the experimental beam to inform it. A cantilever element generated in MATLAB[®] with a hundred nodes represents the beam. This model follows Euler-Bernoulli Beam Theory. Each node of the model represents a cross section slice of the beam and may only move laterally along the beam's weak axis. Larger lump masses apply at the tip and one third location to account for the effects of the sensors on

the beam's dynamic response. Figure 4-3 presents a representation of the beam as a series of lump masses overlaying the cantilever specimen.

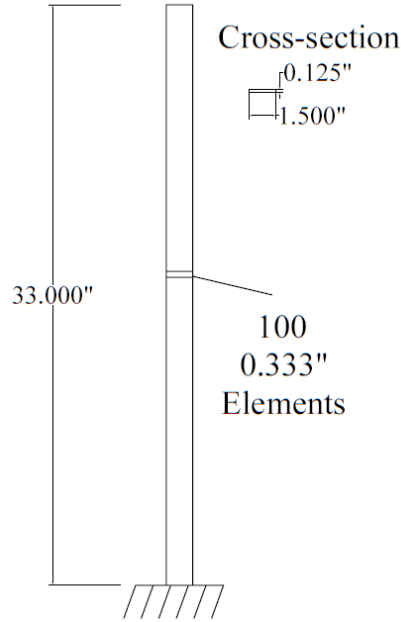


Fig. 4-3: FEM Representation

The study calculated the TRFs of the FE model of the simple structure with the following expression:

$$H(\omega) = \frac{S_{XY}}{S_{XX}} \quad (4.1)$$

, where the H is a Transfer Function, ω is each frequency line, S_{XY} is the cross-spectral density of the input force and the output response, and S_{XX} is the auto-spectral density of the input force. In a continuous domain, the cross-power density is given by the equation:

$$S_{xy}(\omega) = \sum_{m=-\infty}^{\infty} E\{x_n y_{n-m}^*\} e^{-i\omega m} \quad (4.2)$$

, where x_n and y_n are two jointly stationary random processes, $-\infty < n < \infty$, $E\{ \}$ is the expected value operator, and i is the square root of -1.

The study conducted a test without the restraint attached as a pure cantilever beam to update the FE model of the simple structure. From this test the study obtained an experimental damping factor by using the Log Decrement Method. This damping factor was then assumed to be a constant, universal coefficient for the FEM, despite the fact that damping does vary with frequency. This test is comprised of striking the structure with an impact hammer at the 1/3rd location. Each test consisted of three independent strikes to the beam with a sampling rate of 8192 Hz. Since using a hammer excitation generates a zero at the frequency $f=1/T$ Hz, where T is the duration of the hammer impact, the average of these tests comprised the resultant TRF. It is worth mentioning that each of these three tests returned very similar results, especially when compared to the changes present when moving from a simple to complex structure.

The recorded data channels consisted of the impact hammer and the accelerometer at the 1/3rd height (same location). The FEM Mass Matrix implements the masses of the sensors and their connective plates as additional lump masses. It is worth mentioning that this experiment was conducted prior to attaching the stinger to the simple beam.

Table 4-1 shows the comparison of the simple cantilever structure between the FE model and the experiment, displaying the modal masses and the modal frequencies. The calculation of the Modal Masses used the un-normalized values of the modes, obtained from a 276-node model. The study normalized the mode shapes only for visualization purposes using the top DOF as the denominator and presenting a 2DOF mode shape for better comparison with the experiment. The two accelerometers were attached at the tip and 1/3rd height, respectively, since the simple model needs to represent a portion of the complex model. The errors of the frequencies of the first four modes of the structure are

all under 2%, except for the fourth natural frequency which is 2.71%. Table 4-2 also displays the damping associated with each mode, while Figure 4-4 presents the mode shapes.

Table 4-1: Natural Frequency Comparison (Hz)

	Modal Mass (kg)	Modal Mass (%)	MATLAB® FEM Mode Frequency	Experiment Mode Frequency	Frequency Difference	Frequency % Error
f_1	0.57	63.58	2.93	2.90	0.03	1.03
f_2	0.21	22.86	18.13	17.93	0.2	1.12
f_3	0.06	6.53	50.08	49.87	0.21	0.42
f_4	0.02	2.54	106.20	103.4	2.8	2.71

Table 4-2: Modal Damping Comparison (%)

	MATLAB® Finite Element Model	Experiment Results	Difference	% Error
f_1	2.37	2.22	0.15	6.82
f_2	0.38	0.38	0.00	0.18
f_3	0.13	0.14	0.00	-2.18
f_4	0.07	0.07	0.00	-1.66

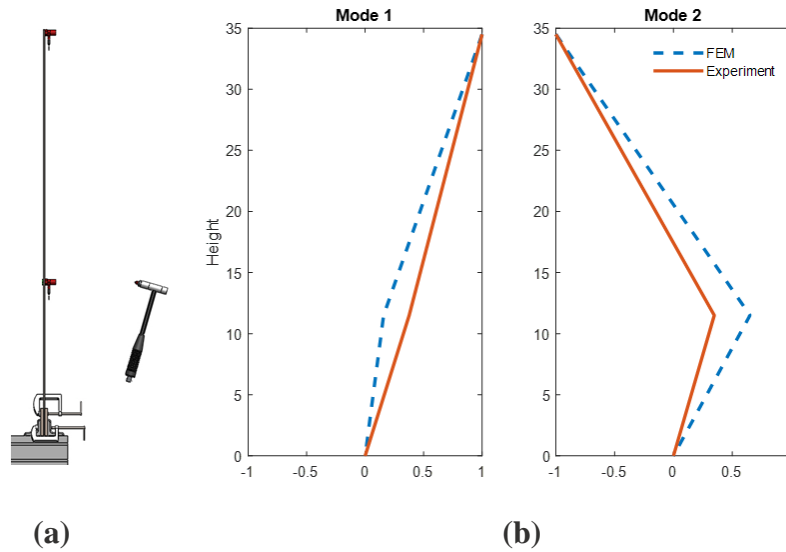


Fig. 4-4: Simple Case Mode Shapes: (a) 2D View of Experiment; (b) Comparison of Experimental and FEM Modes 1 and 2

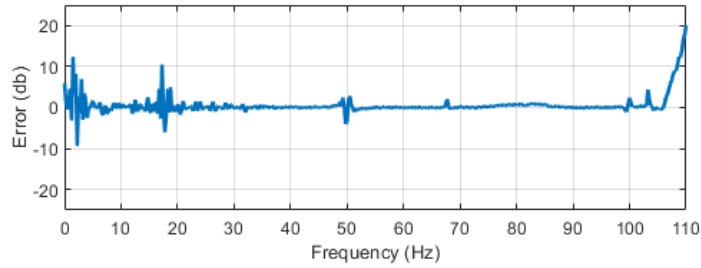
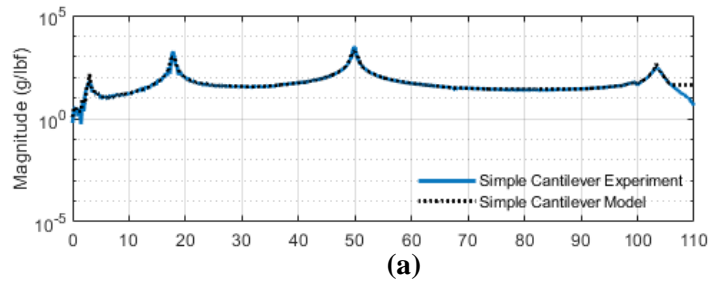
4.2.3: FE Model Update

This study updated the TRF from the simple model between 0 and 110 Hz applying Dynamic Time Warping to ensure peak and pole alignment between the model and the experiment for the first four modes. The error between the estimated and the experimentally measured TRFs of the simple structure evaluates the validity of the simple model. The following equation quantifies the difference between two TRFS using the decibel error [43];

$$Error = 20 \log_{10} \left(\frac{TRF\ Estimate}{TRF\ Standard} \right) \quad (4.3)$$

, where Error is the error metric for a given frequency line, the TRF Estimate is the estimate for that line, and TRF Standard is that of the ground truth. In this case, TRF standard is always the TRF obtained directly from measured outputs of an experiment. Across a range of frequencies, the error is the average absolute decibel error of those frequencies.

Figure 4-5 compares the TRF from the FE model of the simple structure and the experiment with the simple structure at 1/3rd of the height, with respect to an input force at the same location. Figure 3-4(a) shows the TRF amplitudes of both the model and the measured experiment. Figure 3-4(b) shows their decibel error. The largest errors in the TRF of the model of the simple structure are in the regions near the peaks and poles, with a maximum error of 3.3 dB outside these regions. The average error between the TRFs of the dynamic model and the experiment is 0.85 dB between 0 and 110 Hz. This study prioritizes maintaining the fidelity of the peaks in the model of the simple structure and chooses this model for the derivation of the complex experiment estimation.



(b)

Fig. 4-5: Model Vs. Experimentally Measured TRFs at 1/3 Height (a) Magnitude (b) Decibel Error

The study used this model to estimate the dynamic properties of the complex structure by combining it with the results of one SISO experiment, as described in the next section.

4.2.4: Research Methodology

The objective of this chapter is to develop a method that estimates the TRFs of unmeasured locations on a complex structure. The method achieves this by combining the finite element model of a simple structure with the results of a SISO complex structure test. This offers a tool to use in designing experiments which eliminates the need to create a full model with the complex structure and is more versatile than experimentally creating a modal model. Figure 4-6 summarizes the proposed methodology, demonstrating how a simple FEM model is combined with a complex experiment to yield TRF estimates for all output locations.

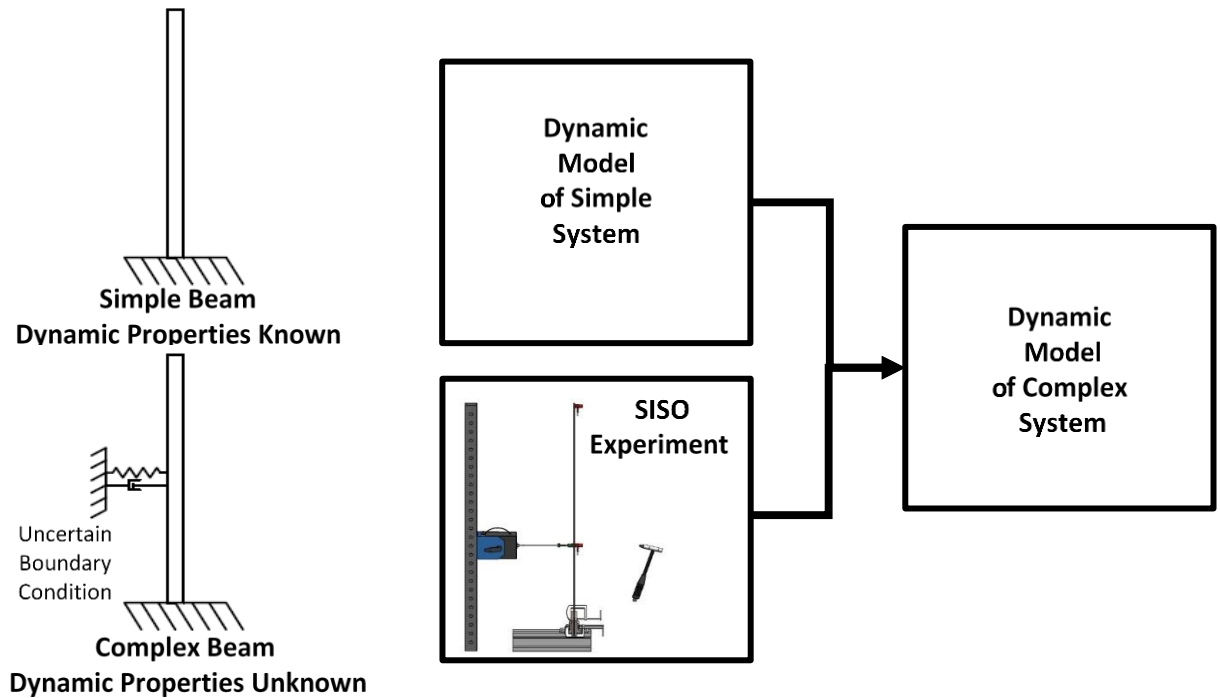


Fig. 4-6: Combining the FEM of a Simple Structure with a SISO Experiment

This method assumes that the system is fully linear; the restraint exerts only an axial force with no rotational or translational effect; and that the dynamic model of the model of the simple structure is an accurate representation of the simple system.

4.3: TRANSFORMATION DERIVATION

4.3.1: Boundary Condition

In the example this thesis presents, an impact hammer actuates the beam at the same location that the restraint was connected to the structure. An accelerometer collects the response on that same location. The possibility of limited experimental access is one of the motivations for developing this method as a first step to enable a new experimental technique. In a more complex example where the input is not at the same location, more terms are involved but the derivation process remains the same.

This experiment used a load cell between the stinger and the beam to measure the force the inactive stinger applies. The methodology makes assumptions about the relationship between the force of the stinger and the input force, and the study used this data channel to validate those assumptions. The presence of the load cell is omitted from descriptions of the experiment in the rest of the thesis since the details of this validation step are not critical and the method is developed for the case where there is no load cell at the tip of the stinger.

This derivation assumes linear superposition and considers the effects of the stinger to be a dependent input to the structure. With this assumption, a TRF of the simple structure with respect to the input force is identical to the TRF of the complex structure with respect to the combined input force from the hammer and reactionary force applied by the stinger. Assuming the use of a model representative of the simple structure, the expression for the output of the complex structure within the frequency domain is then:

$$A = H_{Mod} * (F_{Ham} + F_{LC}) \quad (4.4)$$

, where A is the Fourier transform of the output acceleration, H_{Mod} is the TRF from the model of the simple cantilever structure for a single arbitrary location, F_{Ham} is the Fourier transform of the applied input force by the hammer, and F_{LC} is the Fourier transform of the reactionary force of the restraint.

H_{Mod} is distributed between the two forces which constitute the total input.

$$A = H_{Mod} * (F_{LC}) + H_{Mod} * (F_{Ham}) \quad (4.5)$$

This treats the applied input and the reactionary force from the restraint as two separate inputs with their own relationships to the output. The hammer is the only independent input and the reactionary force applied by the stinger consists of a function of

the hammer's input and the system properties. H_{Sting} relates the output force of the restraint to the input force applied by the impact hammer, similar to a traditional TRF:

$$F_{LC} = H_{Sting} * F_{Ham} \quad (4.6)$$

, where H_{Sting} is the experimental TRF of the reactionary force of the stinger to the input force of the impact hammer, as shown in Figure 4-7.

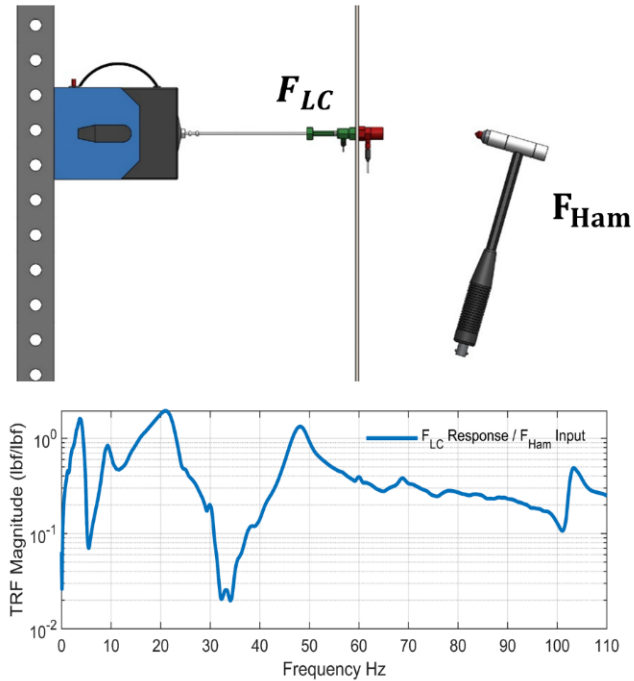


Fig. 4-7: TRF H_{Sting} Description: (a) input and output data sources (b) H_{Sting} TRF Magnitude

Substituting this term into equation (4.4) yields:

$$A = H_{Mod} * F_{Ham} + H_{Mod} * H_{Sting} * F_{Ham} \quad (4.7)$$

4.3.2: Application

Let H_{Test} denote the TRF of the complex structure which relates the output acceleration to applied input force. Dividing both sides of Equation 4.7 by F_{Ham} leaves the definition of H_{Test} on the left. Reorganize the right side of the equation to obtain:

$$H_{Mod} = \frac{H_{Test}}{1 + H_{Sting}} \quad (4.8)$$

This estimates the simple structure TRF based only off of TRFs from the test with the complex structure. Moreover, inverting the expression obtains the TRF of the complex structure with respect to the applied force based upon a model of the simple structure. Rearranging equation 4.8:

$$H_{Test} = H_{Mod} * (1 + H_{Sting}) \quad (4.9)$$

The conversion function developed is independent of the output with no related data channels or TRFs. This indicates that the factor is the same irrespective of the output. As a result, a straightforward test obtains the conversion function without considering the load cell measuring the force applied by the extra connection. Further rearranging to convert the model of a simple structure to represent a more complex one produces Equation 4.10:

$$\text{Conversion Expression} = (1 + H_{Sting}) = \frac{H_{Test}}{H_{Mod}} \quad (4.10)$$

The ratio of the TRFs for an arbitrary DOF is equal to a parameter dependent exclusively on H_{Sting} , which is itself independent of what DOF is considered. This means that the ratio shown is equivalent to the conversion expression for any given DOF, since the relationship stands for a generalized case and the expression it is equivalent to is independent of the DOF chosen. H_{Test} represents a single point. This conversion expression yields an estimate for the TRF of any other point, as according to the equation:

$$H_X = H_{ModX} * \frac{H_{Test}}{H_{Mod}} \quad (4.11)$$

, where H_X is the estimated TRF of a point not measured in the complex experiment and H_{ModX} is the TRF for that point from the simple model. This conversion expression

relates the TRF from a model of the simple structure for any output to the TRF of the complex structure for the same location. With this, researchers can estimate any output of a complex structure using a combination of the FEM of the simple structure and only one SISO experiment. The equations describing this transformation are applicable to the example structure with the Single DOF (SDOF) alteration. This process applies to any location, but it works exclusively for the test setup in which the initial SISO test is performed; if the attachment location is altered between any of the steps, the method is no longer valid. This presents a Single-Input method, but in the future researchers can apply techniques such as superposition to build on this method in Multiple-Input systems, allowing for the safe prediction of experimental responses in MIMO experiments. The following section describes the experiment which this study conducted to validate this method and examine its accuracy and limitations.

4.4: Experiment and Results

An experiment obtained data for the estimation and validation of the estimate. The process presented in the Methodology then used this data to estimate a TRF for the complex structure. This study used the TRF calculated for the same location in the experiment to validate this estimate.

4.4.1: SISO Experiment

The research performed three tests. Each of the experiments consisted of one strike to the beam with a hammer at the 1/3rd location, allotting 15 seconds per strike to record the full vibration. This test used a sampling rate of 8192 Hz for all channels in the experiment. The data channels were: the impact hammer, the accelerometer at the 1/3rd height to estimate

the tip TRF, and the accelerometer at the tip used to validate the estimation. Figure 4-8 shows the experiment.

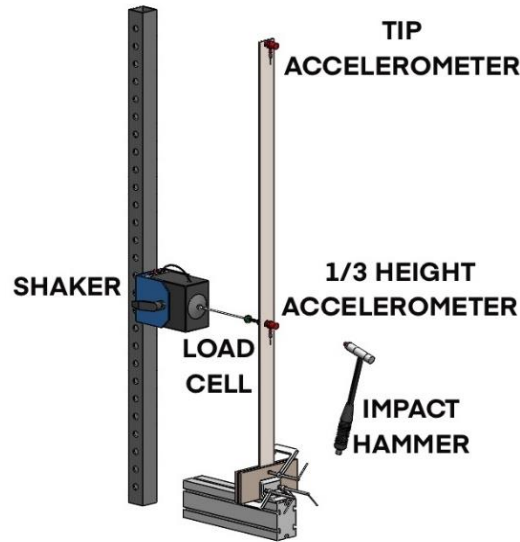


Fig. 4-8: Experiment with Complex Structure

4.4.2: Complex Structure Measured TRF

The average of the three impact events obtains a TRF using the data from the tip accelerometer. This TRF is the ground truth to compare with and validate the new method. The contribution of the new method is that in experimental implementation the research team does not need to install an accelerometer at every location where the TRF is of interest. They can instead estimate the TRFs of these locations with only one SISO test in combination with the finite element model of the simple beam.

4.4.3: Complex Structure TRF Estimation

The study obtained the conversion expression by calculating the ratio of the TRF from the FEM of the simple structure at 1/3rd the height with the TRF from the complex structure using the data from the accelerometer for the same location. This constitutes the conversion factor applied to the finite element model of the simple structure. By using this conversion

factor with a FEM of a simple structure, researchers can estimate the TRF of the complex structure at any output location. For simplicity, the study validated the TRF estimation at the tip of the complex structure with one accelerometer. The Estimate and the Measured TRFs each use one of the two sensors in their formulation. The Estimate and the Measured TRFs each use one of the two sensors in their formulation intentionally for estimation and validation, respectively. For estimation purposes, the study used the first sensor to obtain the single TRF from an impact hammer experiment to estimate any TRF of the entire complex structure. For validation purposes, the study used the second sensor to obtain a metric of error by comparing the results vs. the estimation. The main contribution of the proposed method is that with a simple impact TRF, a different TRF from a different location can be estimated. It is worth mentioning that this TRF has been estimated without using the data from the accelerometer at the tip of the beam.

4.4.4: Results and Analysis

The analysis of this study compared the TRF estimation of the complex structure with the experimentally calculated TRF from the tip accelerometer. This accelerometer was present only for the validation of the estimation and is not necessary for the method.

The study divided the TRF error into discrete frequency regions to better analyze the parts of the TRFs and assigned a rating to each region. The regions were all multiple of 5 Hz increments and if two regions had the same rating they were combined. Each region was rated based on the mean and maximum errors simultaneously within certain dB error ranges, assigning the lower rating of the two if they disagreed. Good rating corresponds to mean and maximum errors below 2 dB and 4 dB, respectively. Fair rating corresponds to mean and maximum errors ranging between 2 to 4 dB and 4 to 8 dB, respectively. Poor

rating corresponds to mean or maximum errors above 4 dB and 8 dB, respectively. The thesis analyzed the estimate TRF first by performance over these regions, and then by the performance at natural frequencies.

Figure 4-8 shows the results of comparing both the estimated and experimentally measured TRFs for the beam response at its tip with respect to an input force at 1/3rd height of the structure. Figure 4-9(a) plots the estimate and measured TRFs together, while Figure 4-9(b) shows the decibel error between them shading each region according to their rating.

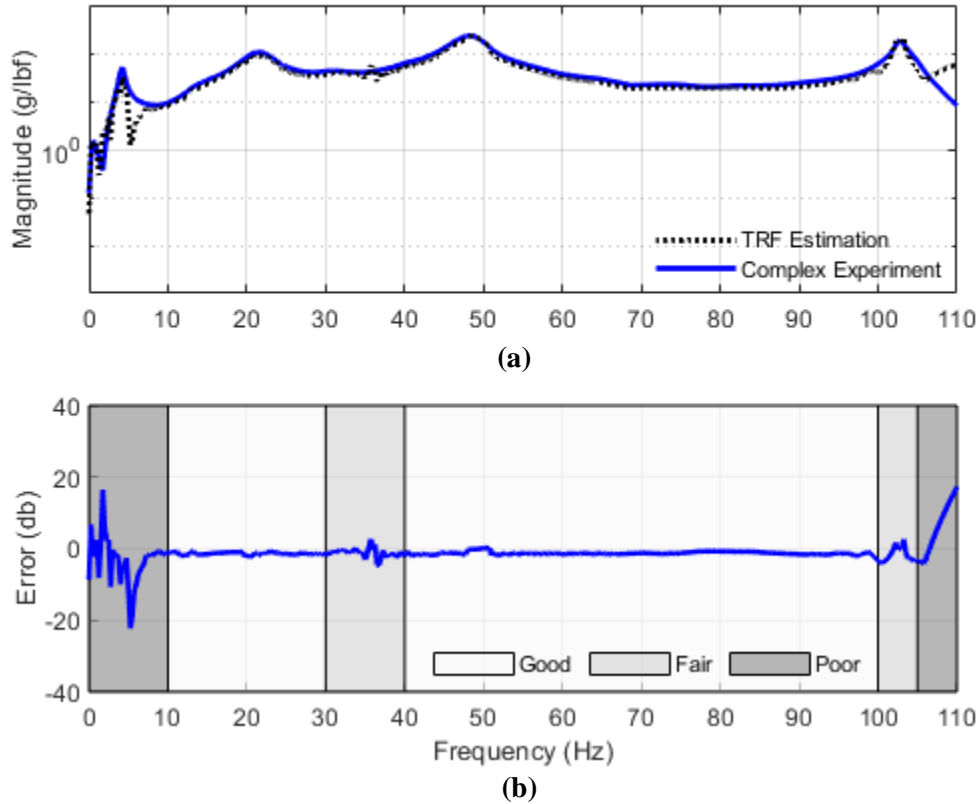


Fig. 4-9: Estimated vs. Experimentally Measured TRFs at Tip (a) Magnitude (b) Decibel Error

In general, the TRF estimation tends to slightly underestimate the experimental TRF of the the complex structure. Table 4-3 shows the mean and maximum errors for each region.

Table 4-3: Comparison of Estimated and Measured TRFs Frequency Ranges

Frequency (Hz)	0-10	10-30	30-40	40-100	100-105	105-110
Mean Error (dB)	5.08	1.36	1.45	1.27	2.29	7.43
Max Error (dB)	22.26	2.52	4.65	3.41	4.08	17.28
Interpretation	Poor	Good	Fair	Good	Fair	Poor

The dB error between the 10-30 Hz range and 40-100 Hz has a rating of good. This includes natural frequencies 2 and 3, and it is worth noticing that the error of natural frequencies 1 and 4 is also low but their vicinities have either fair or poor estimations. For the frequency regions 10-30 Hz and 40-100 Hz, it is also important to note that the mean error has a similar magnitude to the maximum error. This indicates that the error is stable within these regions. The 0-10 Hz region rates poor for TRF estimation, with the largest error of 22.26 dB at 5.25 Hz. This error occurs immediately after the 1st mode located at 4.25 Hz and misrepresents the estimated TRF. The 30-40 Hz region rates fair, with a maximum error of 4.65 dB at 36.75 Hz. This is the location of a pole in the simple system TRF for the 1/3rd height point. The 105-110 Hz region rates poor with a maximum error of

17.28 dB at the last point of the TRF (110 Hz). Finally, for the entire range of 0-110 Hz, the TRF estimate mean and maximum errors are 1.99 dB and 22.26 dB, respectively.

Table 4-4 shows the natural frequencies of the estimated and measured TRFs respectively, describing the frequency, damping, and magnitudes for each mode, while Figure 4-10 presents the first two mode shapes.

Table 4-4: Comparison of Estimated and Measured TRF Natural Frequencies

	Mode 1			Mode 2			Mode 3			Mode 4		
	Exp	Est	Error									
Frequency (Hz)	4.25	4.25	0%	21.5	21.5	0%	48.25	48.25	0%	102.75	102.5	0.24%
Damping (%)	6.79	12.98	91.96%	1.86	2.1	12.9%	0.87	1.03	18.39%	0.37	0.21	43.24%
Magnitude (g/lbf)	52.49	30.95	4.42 dB	105.2	85.41	1.81 dB	231.7	226.1	0.21 dB	186.8	190.8	0.18 dB

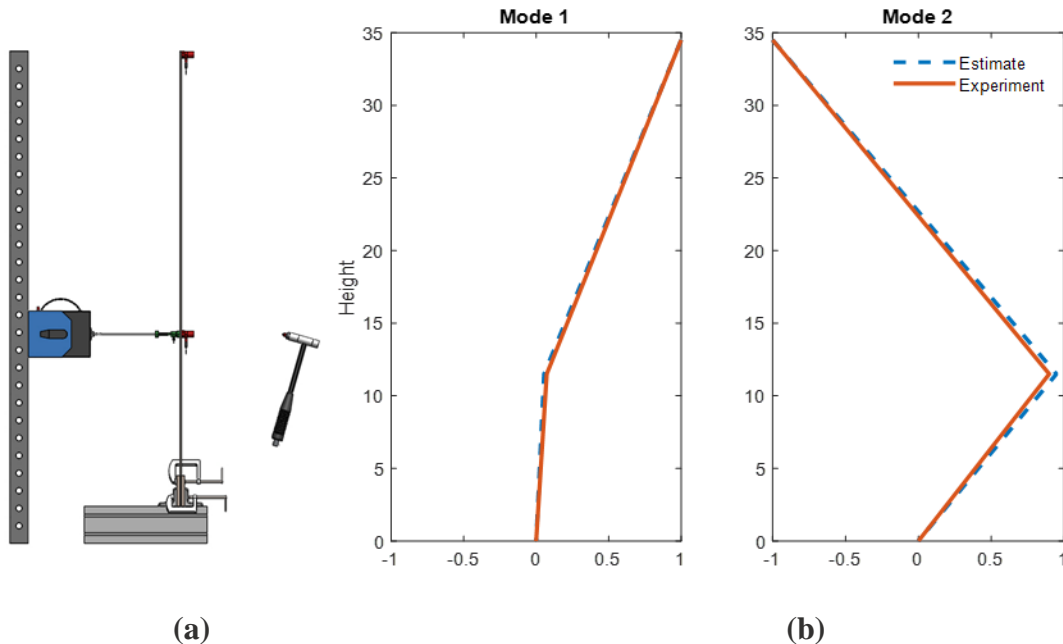


Fig. 4-10: Complex Case Measured and Estimated Mode Shapes: (a) 2D View of Experiment (b) Comparison of Experimental and Estimated Modes 1 and 2

The natural frequencies from the estimated TRF match those of the measured TRF, with the exception of the 4th mode with a 0.25 Hz discrepancy. The damping of the estimated TRF for the 2nd and 3rd modes is good, at 12.9% and 18.39% error respectively. The damping of the 1st and 4th modes match poorly, at 91.96% error and 43.24% error respectively. For the first three modes the TRF estimates a higher damping, except for in the 4th mode which is lower. The damping in the 1st mode has error in the model of the simple structure as well, with the model underestimating the damping of the system. The error of the damping in the 4th mode could be due to high frequency non-linearities. The magnitudes of the modes of the estimated TRF generally match those of the measured TRF. The 2nd, 3rd, and 4th natural frequencies have a rating of Good, with errors of 1.81, 0.21, and 0.18 dB respectively. The 1st mode only has a rating of fair at 4.42 dB. The peaks are the most important part of a TRF and represent the highest priority when addressing errors.

The large errors in the TRF estimation in the first and fourth mode coincide with the large errors in the model of the simple structure. Comparing Figures 4-5 and 4-9 make it easy to observe how the TRF deviations occurring between the Measured and Estimated case correlate with those between the measured Simple case TRF and the simple model. The discrepancies in the Estimate which correlate with those in the simple model dominate the error, suggesting that this underlying fault is the greatest overall source of error in this example of the proposed method. This correlation is unsurprising given the formulation of the estimation as the result of using data from a combination of a complex case experiment and a simple case model, as proposed in the Methodology. This manifests most as the error within 0-10 Hz and 105-110 Hz which is shared by both systems. A shared error occurs at 36.75 Hz as well, where the simple structure TRF also has a pole. This correlation occurs

for the largest errors in the estimation, indicating a relevant relationship between the two TRFs. This emphasizes the importance to this method of ensuring an accurate model of the simple system to build on, as errors present in the resultant TRFs will propagate through the proposed method. Deviations in boundary conditions are also a potential source of error. An unexpected boundary condition in the test could offset the results. Furthermore, the method is reliant upon the applied boundary condition working exclusively in the axial direction of the stinger- the lateral stiffness present represents an unaccounted for effect of the imposed boundary condition on the structure. The applicability of the estimated model is only valid insofar as the simple FEM represents the simple case experiment, and that the only change between the simple and complex case is the attachment of a partial transverse restraint with zero stiffness in other DOFs.

These results constitute the first step to enable researchers to efficiently estimate the unmeasured TRF for any output of a complex structure using only the finite element model of a simple structure and a SISO experiment.

4.5: Conclusions

This chapter measured the error between the estimated and the measured TRFs. The method proves to be accurate for most of the natural frequencies within the frequency range the study examined. Based on these results, the study concludes that the method helps efficiently estimate the unmeasured outputs for a cantilever beam with a partial transverse restraint. While more accurate methods of determining TRFs for test-planning exist, this method presents advantages in certain settings. Typically, methods to perform a pretest analysis with a complex structure involve either a FE model representing the entire system, or the generation of a modal model with an experimental process. As compared to using a

pure FE model, the proposed method does not require knowledge of the boundary condition's dynamic properties. Additionally, this method also has advantages over experimentally making a modal model, which necessitates the application of a sensor at every relevant output. This can be expensive, and by its nature imposes a change on the dynamic system by the addition of the sensor mass. However, the method presented only requires one measured output while still estimating the TRF of any other output, offering the versatility of a full model. This project estimates the unmeasured TRF of a complex structure with an uncertain boundary condition by transforming a model of a simple structure with data obtained from one SISO experiment with the complex structure. However, the same process can apply to more complex situations as well, with more boundary conditions or other input locations.

Chapter 5: New Methodologies to Identify and Correct the Misplacements of Sensor Location in Experimental Dynamics

5.1: Introduction

This chapter investigates the estimation of the location of a sensor given the output data of a physical experiment. The research does this with two different methods. One of these is by combining the modal contributions of the system at a range of frequencies with the frequency domain input signals to quantify and use the modal involvement of a given signal. The other method performs a model-matching technique by exclusively changing the positions of the sensors in an FEM to find what model placement results in the most similar natural frequencies to the observed experiment. This thesis demonstrates the ability of these techniques to detect the misplacement of a sensor. Since the methods rely on detecting changes in the dynamic properties, it will be most effective in experiments where the mass of the sensors relative to the mass and stiffness of the structure are not insignificant, while offering little insight for large, very stiff structures with small, light sensors. This technique potentially allows for the correction of sensor placement errors in a physical experiment.

5.2: Methodology

This chapter investigates two different methods for identifying sensor location error. These two methods are the use of modal contributions, and the use of a model-matching technique. Applying the model-matching technique has potential to be more precise than using modal contributions, informing the operator what the magnitude of the sensor placement error is. Conversely, the modal contribution method offers more insight to how

a given sensor misplacement will result in error and can help the operator in the initial test-design process to help minimize the effect of a sensor misplacement. These two methods are illustrated in Figure 5-1.

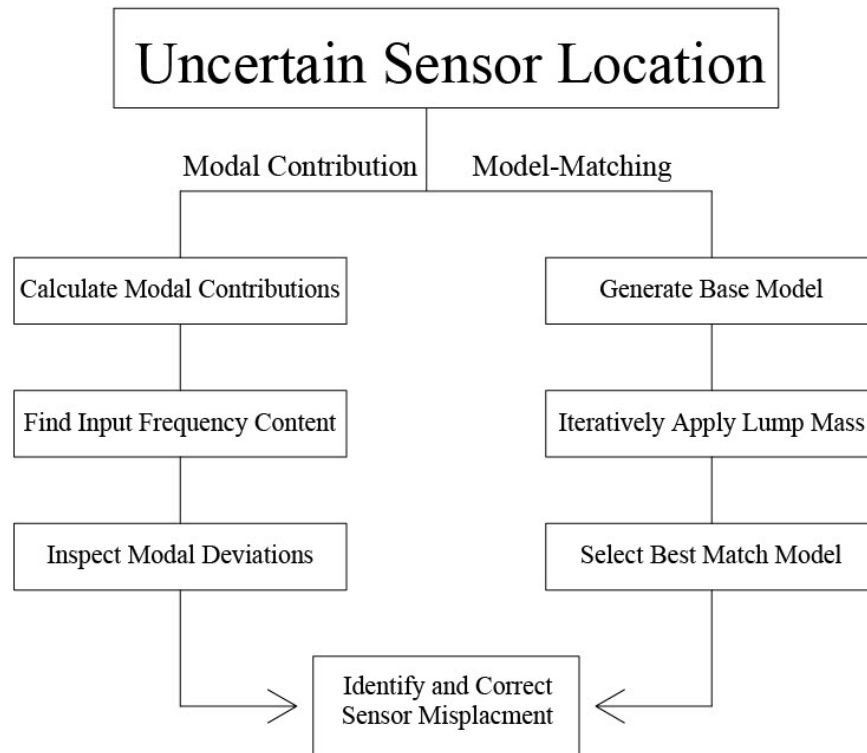


Fig. 5-1: Two Methods for Detecting Sensor Placement Error

5.2.1: Modal Contributions Method

This chapter examines some errors within the context of Modal Contributions, to establish which modes are most relevant for a given frequency, how that will affect the results, and how this can inform a researcher in performing an experiment. Researchers traditionally use Modal Contributions for Modal Superposition, whereby the force vibration response for a given input is estimated as a combination of different mode shapes at different magnitudes. By their nature then, Modal Contributions indicate the extent to which each

mode is relevant for an input at a given frequency. Using Modal Superposition, a force vibration response is summed by Equation 5.1 which is illustrated by Figure 5-2.

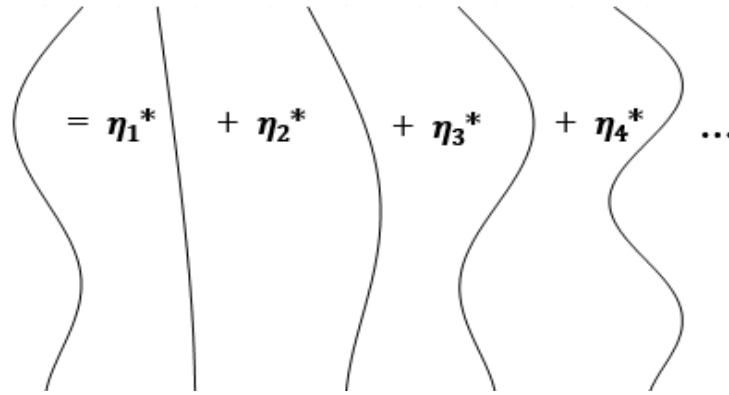


Fig. 5-2: Modal Contribution Application

$$y = \sum \eta_i \Phi_i \quad (5.1)$$

, where y is the response estimate, η_i is the modal contribution factor for mode i , and Φ_i is the mode shape of mode i . Putting the equation into matrix form and rearranging, one can solve for η for each frequency, given the force vibration response:

$$\{\eta\}_j = [\Phi]^{-1}\{y\}_j \quad (5.2)$$

, where $\{\eta\}_j$ is the vector of Modal Contribution Factors corresponding to a vibration at frequency j , and $\{y\}_j$ is the relative force vibration envelope for a vibration at frequency j . In practice, the study only used the first ten modes due to the negligibility of further within the frequency domain examined.

This research estimates the force vibration response envelope by inputting a BLWN at the one third point in a model simulation and using the responses to estimate the TRFs of each node along the beam. The magnitude of these TRFs at a given frequency then represent the relative response experienced at that frequency, resulting in the force

vibration response used to find the Modal Contributions. Researchers did this at 1 Hz increments from 1 to 200 Hz, calculating the percentile Modal Contributions at each frequency as illustrated in Figure 5-3.

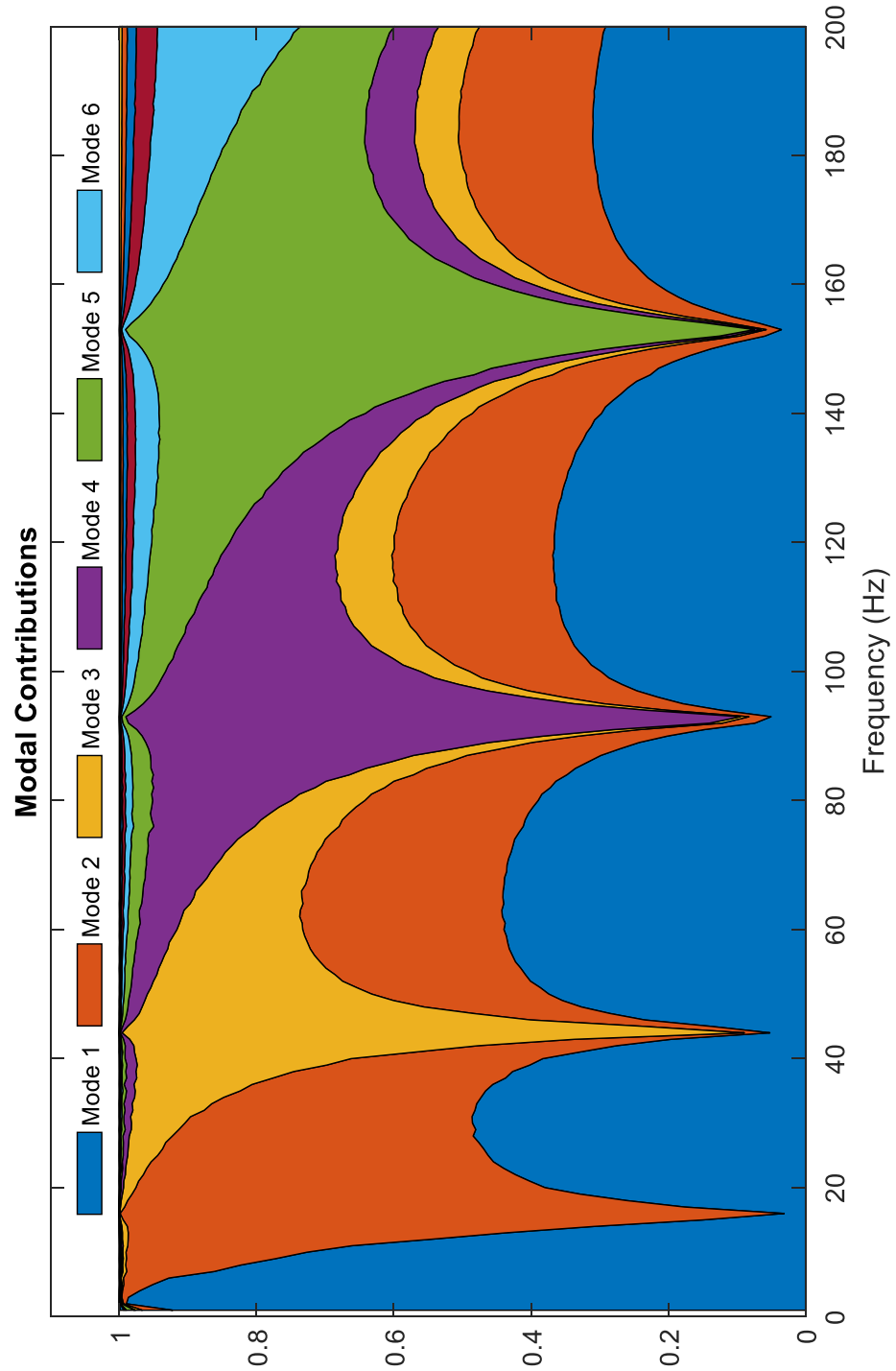


Fig. 5-3: Modal Contributions

This chapter combines the modal contributions with the frequency spectrum of broadband input signals to justify patterns in dynamic response error by investigating mode sensitivity to sensor location.

5.2.2: Model-matching Method

This thesis also performs a model-matching process similar to a sensor based Finite Element Model Update (FEMU) using the natural frequencies found in the experiment as the standard for matching dynamic properties. The base FEM represents the beam with no sensors attached, while the update iteratively placed discrete lump masses representing the sensors at different locations along the beam at $1/16^{\text{th}}$ of an inch (0.15875 cm) intervals. By design, these intervals coincide with the distribution of the 552 nodes which comprise the beam representation. Unlike a traditional FEMU, this process focuses on using a model to identify an error in the physical setup so it can be addressed, whereas most FEMUs are designed to fit the model to the experiment.

In this thesis, this model-matching process focuses on determining the location of the one sensor which the experimental process deliberately placed at different locations. A series of experiments quantify the dynamic response of the beam at each sensor location. A series of Finite Element Models (FEMs) then generate the theoretical dynamic responses for a wide array of sensor locations by applying a lump mass representative of the sensor at varying heights along the beam. For each sensor location tested after the sensor lump masses were applied, this study compares the first five eigenvalues of the FEM system with the first five modes found in the physical experiments. This chapter investigates three metrics to score the model location setups. Each of these metrics indicate how much the

model natural frequencies differ from the experiment, with a score of 0 indicating a perfect fit for the first five modes. Equations 5.3, 5.4, and 5.5 define these parameters.

$$Total\ Deviation\ (TD) = \sum_{i=1}^5 |Exp_i - Mod_i| \quad (5.3)$$

, where Exp_i is the frequency of mode i as found in the experiment, and Mod_i is the frequency of mode i as taken from the eigenvalues of the FEM for a given sensor location setup.

$$Maximum\ Deviation\ (MD) = \max (|Exp - Mod|) \quad (5.4)$$

$$Total\ Relative\ Deviation\ (TRD) = \sum_{i=1}^5 \left| \frac{(Exp_i - Mod_i)}{Exp_i} \right| \quad (5.5)$$

This study defines the sensor location setup with the lowest metric to be the location estimated by the model.

5.3: Experiment

5.3.1: Physical Setup

This study examines a 34.5x1.5x1/8th inch (87.63x3.81x0.3175 cm) steel cantilever beam with two piezoelectric accelerometers magnetically attached to the specimen at the tip and at one third the height. The study placed the one third sensor at three primary locations, although simulations also investigated other locations. These were 7/16th of an inch (1.111 cm) above the one third point, precisely on the one third point, and 7/16th of an inch (1.111 cm) below the one third point, designating them as the Up, Centered, and Down cases, respectively. The experiment used the interval of 7/16th of an inch for continuity with other research which is not relevant to this thesis. The beam is excited by a stinger-based actuator, which connects to the beam at one third the height with no variation in location.

The sensor and magnetic plate assemblies each have a mass of 0.0952 lb-mass (43.2 g).
Figure 5-4 displays a representation of the three setups.



Fig. 5-4: Experiment Setup

5.3.2: Experiment Process

For each of the three physical setups of sensor location, the test excited the structure with a 30-second long Band-Limited White Noise input, ranging from 0 to 200 Hz. The data channels consisted of a load cell attaching the stinger to the beam, the sensor at the tip, and the sensor at one third the height. These tests obtained the TRFs associated with each of the structures, using Equation 6:

$$H(\omega) = \frac{S_{XY}}{S_{XX}} \quad (5.6)$$

, where the H is a Transfer Function, ω is each frequency line, S_{XY} is the cross-spectral density of the input force and the output response, and S_{XX} is the auto-spectral

density of the input force. In a continuous domain, the cross-power density is given by the equation:

$$S_{xy}(\omega) = \sum_{m=-\infty}^{\infty} E\{x_n y_{n-m}^*\} e^{-i\omega m} \quad (5.7)$$

, where x_n and y_n are two jointly stationary random processes, $-\infty < n < \infty$, $E\{ \}$ is the expected value operator, and i is the square root of -1 .

Figure 5-5 presents these TRFs for the tip location with respect to the one third input.

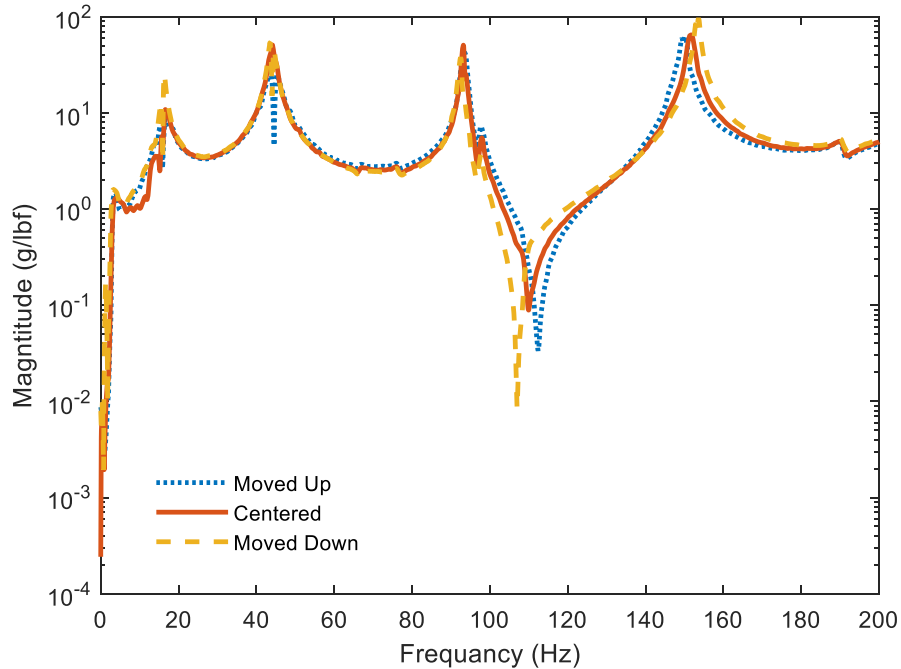


Fig. 5-5: Experiment TRFs

The TRFs have similar peak values at low frequencies, with the deviations increasing as frequencies also increase. There is also a notable deviation in the anti-resonance between the fourth and fifth modes, which seems more susceptible to changes due to sensor placement error than the TRF peaks within this frequency range.

5.3.3: Sensor Location Error Effect

While some deviations between the three TRFs are visible, there are many frequencies at which the naked eye cannot distinguish them from each other. This study performs a simple test to investigate the effects of the sensor movement on the time domain. Figure 5-6 describes the process, illustrating how the test estimated time histories for each sensor location, and compared these with the measured case, for which the sensor was centered. This study conducted the test via simulations so the effects of sensor location could be better isolated from other potential sources of errors. The input forces for each frequency have the same amplitude, so the time history variation in output magnitude is due to the system dynamic properties. The test also assumes system properties to be linear, with respect to parameters such as damping. Figure 5-7 presents a sample of the time histories resulting from the test.

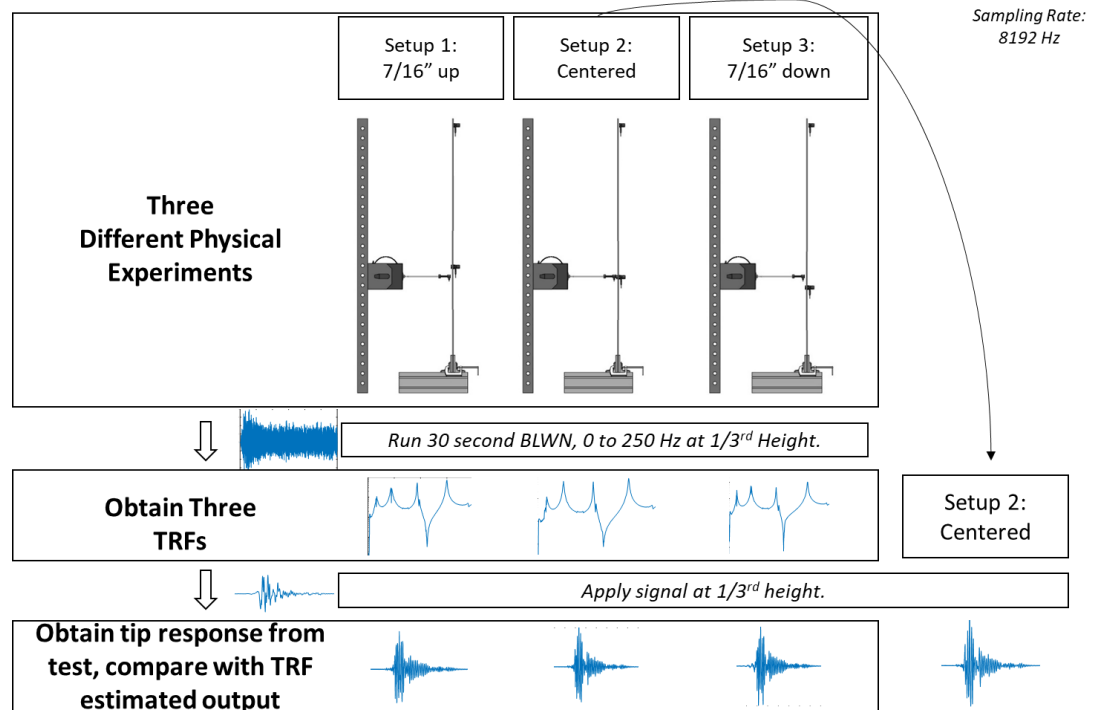


Fig. 5-6: Sensor Location Effect Test

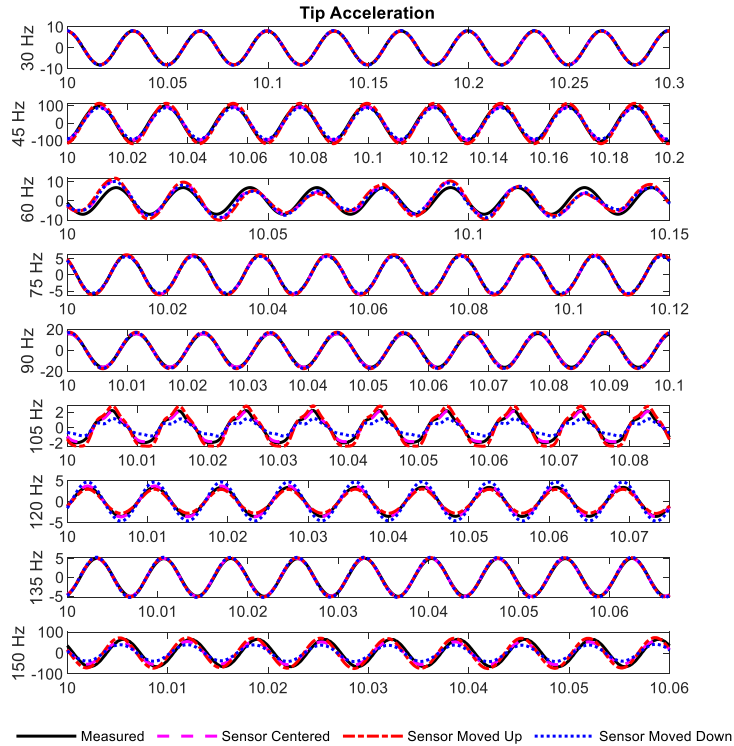


Fig. 5-7: Sensor Location Effect Time Histories

The time histories in Figure 5-7 are normalized with respect to the time domain, such that each frequency window displays 9 cycles. This is to simplify the comparison of each frequency with the others. Inspecting Figure 5-7 reveals that the time histories are distinctly prone to error due to a sensor placement error, even at frequencies where it may be difficult to see a deviation in the TRFs. Figure 5-8 plots the percent error in GRMS values for each of these time histories for a more quantitative comparison. ‘This study uses GRMS values as they provide a simple metric to the overall magnitude of a time history, allowing for estimations of the scale to which two signals vary. The following equation calculates GRMS:

$$GRMS = \sqrt{\frac{1}{N} \sum_{n=1}^N |signal|^2} \quad (5.8)$$

, where signal is the time domain response of the system at a given location for a given input, and N is the number of discrete points in signal. For this study, signal is a 10 second steady state window extracted from the original 30 second test.

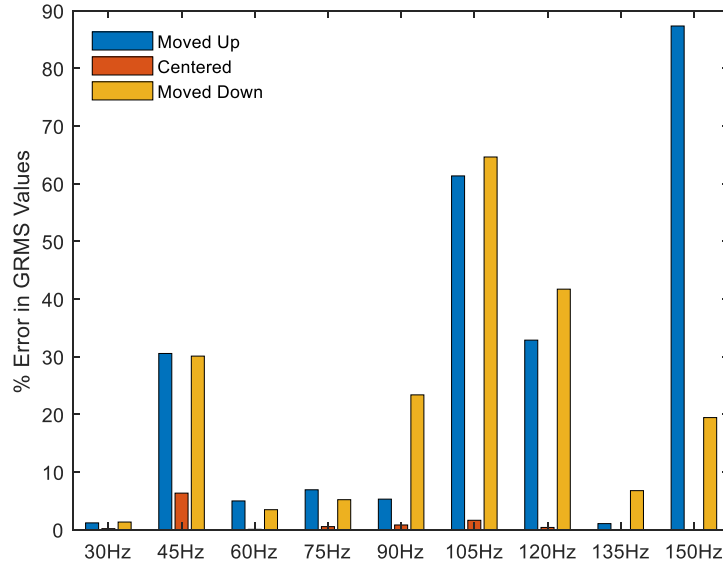


Fig. 5-8: Sensor Location Effect Summary

This plot demonstrates the variable effects of sensor placement error, and how drastic they can be even for a small change in location. Errors in magnitude reached up to 87%, with a mean moved case error of 24%. This emphasizes the importance of ensuring adequate accuracy when placing sensors, and of taking measures such as those discussed in this thesis to correct potential mistakes.

5.4: FEM

The study created a Finite Element Model (FEM) of the cantilever beam using the same geometric and material properties as the experimental beam. This model uses a damping coefficient obtained with Log Decrement method from an experiment, assuming universal damping. The model was created and analyzed within MATLAB®, applying Euler-Bernoulli Beam Theory. An element with 552 nodal elements represents the

34.5x1.5x0.125 inch (87.63x3.81x0.3175 cm) beam, with lump masses located where sensors are centered to account for their effect on the beam dynamics. Each node is a cross section slice of the beam and is constrained to move only in the plane which bisects the broad face of the beam. As a result, the model only considers the bending modes within this plane. Figure 5-9 illustrates this model as a series of lump masses overlaying the beam. It should be noted that these illustrated nodes are not drawn to scale with the dimensions of the beam.

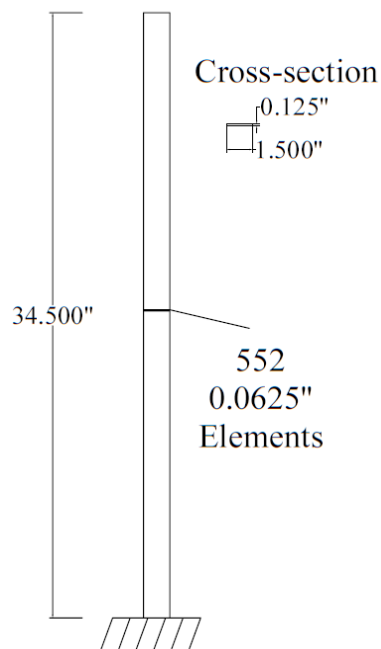


Fig. 5-9: FEM Representation

5.5: Results

5.5.1: Modal Contributions Results

This thesis performs a similar process as was performed with the nine harmonic signals with five different broad-band signals to demonstrate the application of modal contributions. The experiment applied a signal based off the El Centro Earthquake, as well

as four signals based off measured train crossing events on the Bluford bridge, a timber bridge near Edgewood, Illinois [13]. To compare each signal fairly, the research windows the primary excitation event from each signal, as indicated in Figure 5-10. Each of these windows were resampled to have 24,576 points. This allows a comparison of the different signals despite varying time durations. From this point, the analysis is identical to how it is performed with the sinusoidal signals.

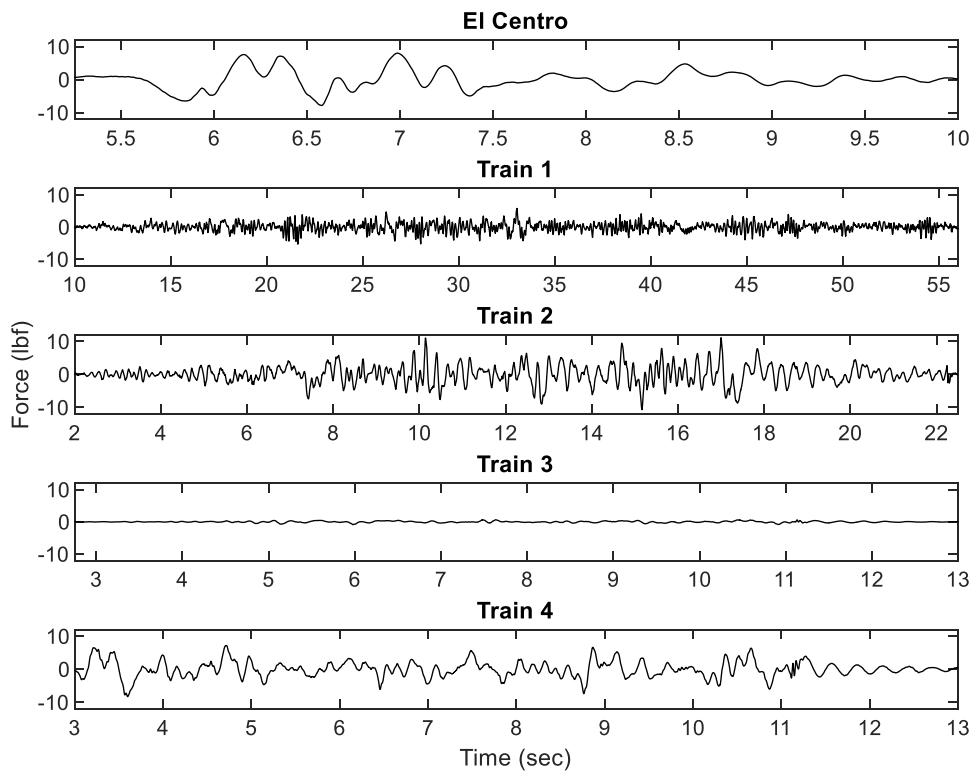


Fig. 5-10: Broadband Input Time Signals

The dynamic time sampling in Figure 5-10 gives the impression of dramatically different frequency contents, but each of the broadband signals are actually similar in frequency range. This is depicted in Figure 5-13. Except for Train 3, each signal is also roughly equal in amplitude, peaking around an absolute value of 10 lbf. Train 3 is much lower, and the analysis includes it to demonstrate that the proposed application remains

viable independent of input magnitude if the other assumptions such as linearity are still met. These signals are those measured in a Centered case physical experiment, which this chapter then implemented as inputs in the simulations. Figure 5-11 displays the results of performing this analysis with both a simulation and a physical experiment case for validation.

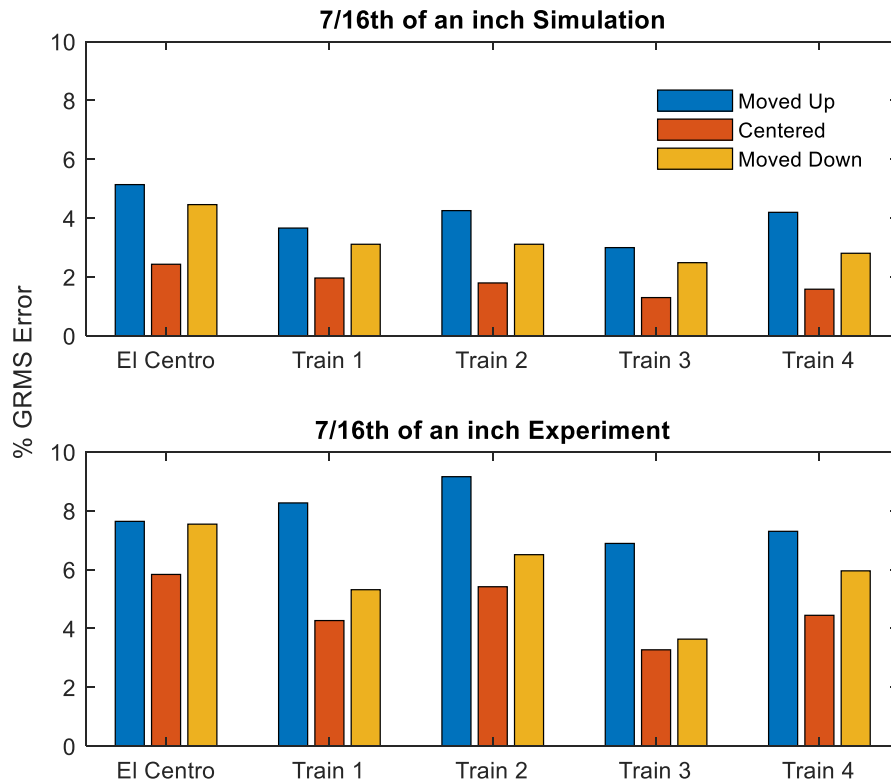


Fig. 5-11: Broadband Input Results: Simulation and Experiment

As expected, and seen in the harmonic signals, the Center case error is consistently the lowest. The physical experiment overall has a higher error than the simulation, which is also expected due to the greater possible number of sources of error. Of interest, the Center case error increases disproportionately as compared to the moved cases. In both the

simulation and physical experiment, the Moved Up case error is more significant than the Moved Down case.

It is of note that the overall magnitude of the error with this metric is notably lower than in the harmonic cases. This is due to the fact that as a given frequency the change in sensor location will have a given effect, either increasing or decreasing the magnitude of the values in the time history. However, in a broadband signal, some frequencies will witness an increase in magnitude, while others will see a decrease. This results in a more stable overall magnitude for the time history.

Train 3 has a very similar magnitude of error to the other broadband tests despite having a substantially lower input magnitude, as seen in Figure 5-10. This indicates that these tests occur within a relatively linear range of the system, as the ratio of the response to input and the effects on the percentage error remain consistent irrespective of the input force level. This also reinforces the relevance of the sensor movement, as even with very small force inputs the sensor location has a notable effect on the error that did not decrease with signal amplitude.

Figure 5-12 presents the results for performing a simulation of the same process at four different sensor deviations with $1/8$ th of an inch intervals. These deviations are $9/16$ th of an inch, $7/16$ th of an inch, $5/16$ th of an inch, and $3/16$ th of an inch. This provides additional validation for trends noted in Figure 5-11, as well as investigating how the error scales with the magnitude of sensor misplacement.

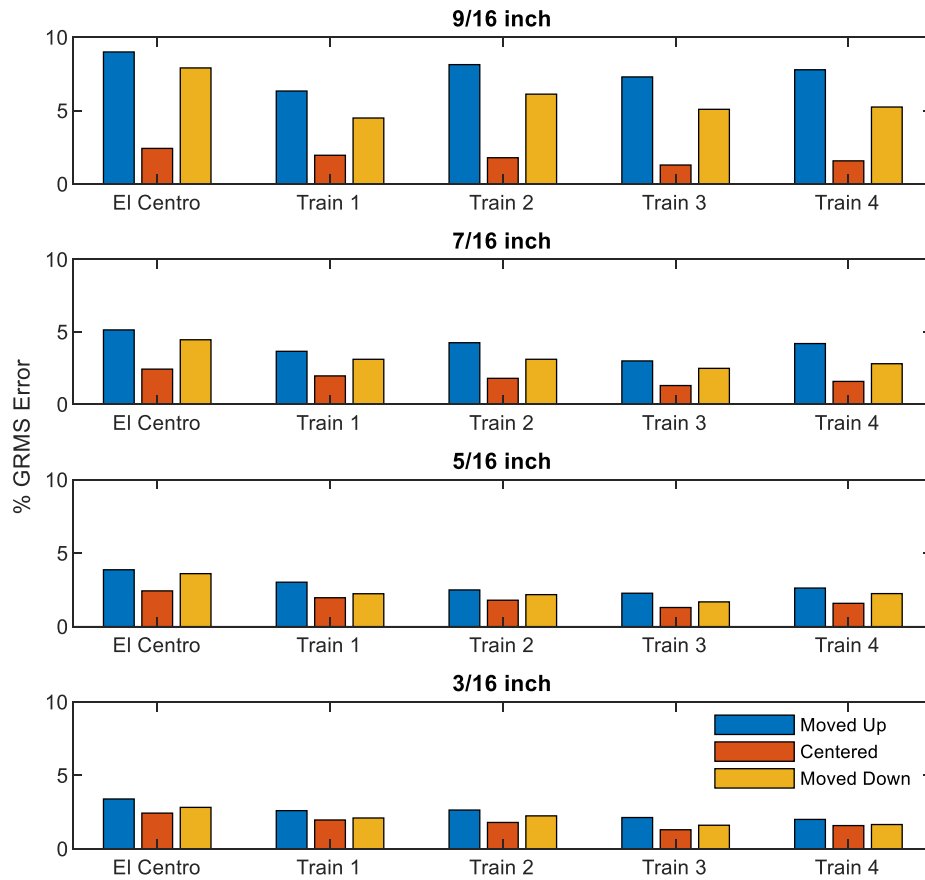


Fig. 5-12: Broadband Input Results: Different Intervals

The patterns observed in the 7/16th of an inch simulation and physical experiment are consistent at the three new sensor location cases. The Centered case error is the lowest of each trio of locations, with the Moved Up case demonstrating more error than the Moved Down case. Additionally, Train 3 continues to have a similar magnitude of error to the other signals, in spite of the significantly reduced input force magnitude.

Looking to modal properties, modal contributions, and the input signal frequency content, the increased errors in the Moved Up case make sense and can be qualitatively predicted. This is due to the fact that the early modes of this structure vary more for an upward movement than a downward movement, and that most of the energy in these

broadband inputs tends to be below 25 Hz, as shown in Figure 5-13. Figure 5-3 illustrates how the dynamic response of this structure is dominated primarily by the first two modes for this range of frequencies.

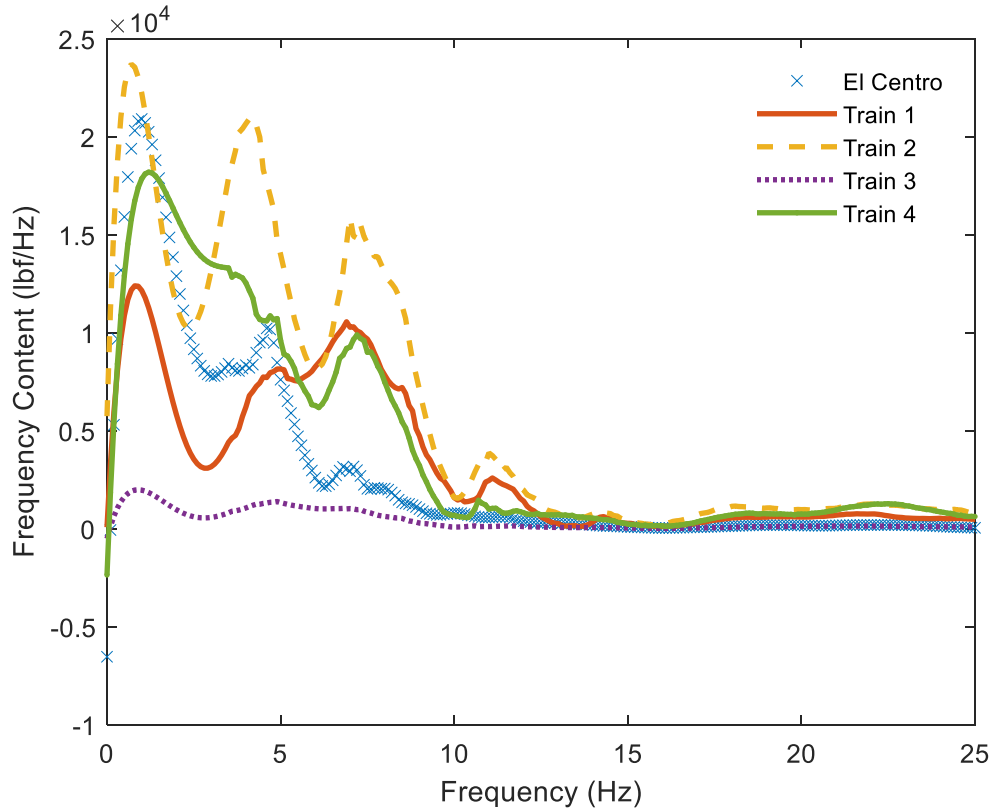


Fig. 5-13: Broadband Input Frequency Domain

The research multiplied the magnitude of each signal at 1 Hz increments by the corresponding Modal Contributions from Figure 5-3, then normalized this product by dividing by the total sum of the result. This is shown in Figure 5-14, which only displays the first 25 Hz due to the negligibility of the higher frequency content. This parameter indicates the degree of relevance each frequency has within the overall input of the signal, as well as to what extent each mode contributes at that frequency.

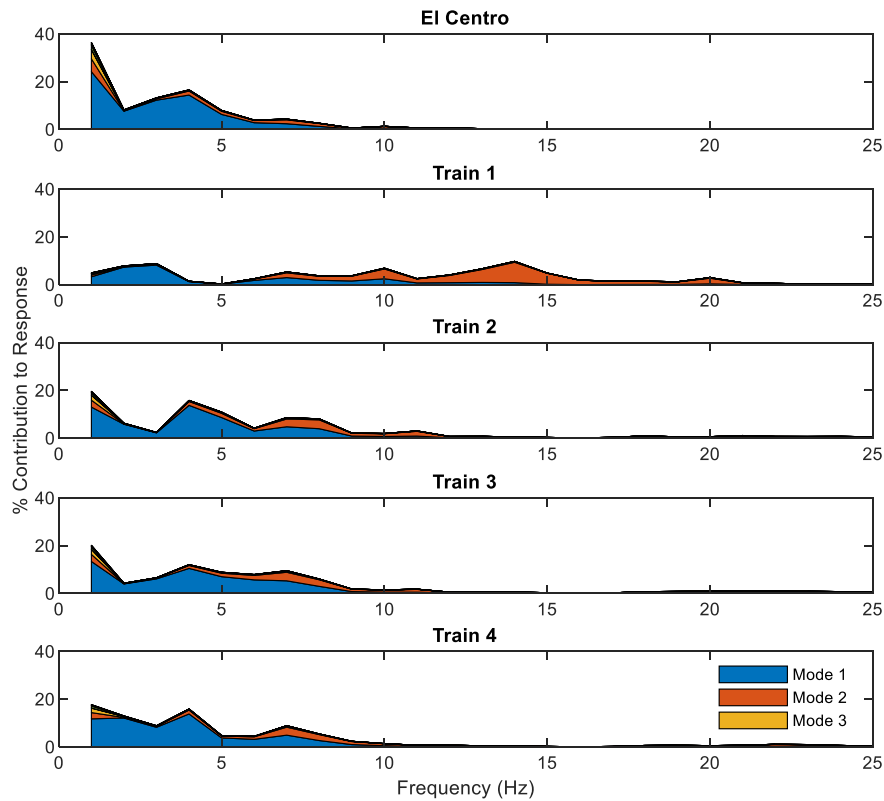


Fig. 5-14: Percentage Contribution to Response

The sum of Modal Contributions at a given frequency then is the same as the frequency domain of the input, normalized with respect to the sum of all energy in the signal. More relevantly, the sum across all frequencies for a given mode represents the total percentage of the input signal that that mode constitutes. Table 1 presents this broadband signal Modal Contribution for the first five modes.

Table 5-1: Broadband Input Modal Contributions (%)

	Mode 1	Mode 2	Mode 3	Mode 4	Mode 5
El Centro	73.3	16.82	6.09	0.48	1.86
Train 1	36.53	48	12.89	1.11	0.84
Train 2	60.55	27.84	8.13	0.84	1.46
Train 3	59.25	28.36	9.09	0.8	1.37
Train 4	63.1	24.62	8.32	0.86	1.91

The first two modes of the beam consistently comprise between 84% and 90% of the input magnitude, quantifying the trend in Figure 5-13 of primarily low-frequency energy dominating these inputs. Table 5-2 displays the extent to which the tip magnitudes for each of the natural frequencies changes with a 7/16th inch change in sensor location. The combination of Tables 5-1 and 2 then justify the sensor location effect trend observed with the broadband signal experiments.

Table 5-2: Tip Response Change (%)

	Up	Down
Mode 1	1.035	0.071
Mode 2	0.816	0.695
Mode 3	4.197	4.022
Mode 4	3.214	6.37
Mode 5	5.837	2.903

This application of modal contribution to explain patterns in error may also help in certain situations where the magnitude of a sensor misplacement may be known, but not the direction. By determining how the modes change and what the anticipated frequency content of a signal is, researchers can predict how a given error in sensor location will manifest in the error. This can also provide an idea of the sensitivity of a system to sensor location which can aid in the initial setup of an experiment. For example, in this case a researcher could look at the theoretical aspects of modal contribution and mode deviations and inform them to err on the side of placing the sensor too low, as small downward deviations are more likely to have a negligible effect on the system dynamics.

5.5.2: Model-matching Results

Tables 5-3 presents the results of applying the sensor-based model-match technique. The table compares the measured height of the one third location sensor with what the method estimates the height to be based on the measured mode frequencies from each metric. The

one third location, at 11.5 inches from the base of the beam, was set as the datum for these comparisons.

Table 5-3: Sensor Placement Error (in)

	Nominal	Total Deviation	Maximum Deviation	Total Relative Deviation
Moved Up	0.4375	0.6875	0.5625	0.4375
Centered	0	0	-0.125	0
Moved Down	-0.4375	-0.6875	-0.875	-1.1875
Total Difference		0.5	0.6875	0.75

The Total Deviation metric scored the lowest and best of the three, with a total absolute discrepancy between the three cases of half of an inch (1.27 cm). Of note, the model update exaggerated the real case, placing the sensor a quarter of an inch (0.635 cm) higher than measured for the Moved Up case, and likewise a quarter of an inch (0.635 cm) lower than measured for the Moved Down case, while placing the Centered case precisely where it should. The Maximum Deviation metric arrived at a closer conclusion for the Moved Up case than the Total Deviation but performed more poorly on both the Centered and Moved Down cases. The Total Relative Deviation placed the moved up and centered case sensors precisely where they should be, but for the Moved Down case placed the sensor $\frac{3}{4}$ th of an inch (4.445 cm) below the measured location.

These results demonstrate the application of a model-matching technique to identify sensor misplacement. Future research may investigate other possible metrics for this process. These other metrics may either involve comparing natural frequencies like those presented in this chapter or may investigate other quantities to compare. Future research may also look into methods to isolate model/physical setup differences to sensor location.

5.6: Conclusions

These results demonstrate the potential in using two different techniques when considering sensor placement error. These two techniques can detect a small movement in sensor location from what was intended and inform the operator as to which direction the sensor should be moved. Applying Modal Contributions and considering input load frequency content comprises one of these techniques, while a model-matching technique is the other. These methods rely on quantifying the differences in dynamic properties of the relevant System Under Test (SUT), rendering them exclusively useful for systems where the mass of the sensor is not negligible with respect to the mass and the stiffness of the system. These methods also depend on having a good model of the base system to begin with. This is important to the modal contributions approach to ensure that the analytical modal contributions are representative of the system, and important to the model-matching technique so differences between the model and the experimental output may be reasonably assumed to be due to a difference in the relevant variable, sensor location. There are many possible metrics which can be used in the model-matching process. Of those considered in this study, Total Deviation performed the best overall. Total Relative Deviation place the moved up and centered cases accurately but was substantially off for the moved down case. The two methods described in this chapter represent the first steps in finding new, effective techniques for identifying and correcting sensor placement error in experiments.

Chapter 6: Conclusions

6.1: Summary

This thesis presents the results of research investigating uncertainty in structural dynamic MIMO testing. It specifically discusses a proposed method for dealing with uncertain boundary conditions in the form of elastic transverse restraints, and two different methods to detect and correct the effects of a small sensor misplacement. The following sections discuss a summary of these results, as well as the current shortcomings in this research and how it relates to future work.

6.1.1: Uncertain Boundary Conditions

Boundary conditions comprise an essential part of models but are difficult to accurately represent, particularly when the dynamic properties are not well understood. One common type of boundary condition is an elastic transverse restraint, such as a highly damped 1DOF spring. This thesis investigates a potential method for transforming the TRF of a simple beam to represent that of the beam with one such attachment. This technique achieves this by using the results of a single SISO experiment to estimate the TRF of any output location along the beam.

To quantify the validity of the proposed method, this study measured the error between the measured TRF at the tip location and an estimate using the proposed technique. The results of this trial indicate that the method is accurate for most of the natural frequencies within the frequency range the study examines. Regions of inaccuracy correlate well with inaccuracies in the original simple model, emphasizing the importance of starting from a good simple model for this process, as errors that are present will propagate through the estimation. Outside of these error frequencies, the estimation had an

error rating of ‘good,’ as the mean error for these regions was below 2 dB, and the maximum error was below 4 dB.

This thesis concludes that the method helps efficiently estimate the unmeasured outputs for a cantilever beam with an elastic transverse restraint, and a similar technique may extrapolate to more complex geometries. While there are more accurate methods of determining TRFs for test-planning, this method presents some advantages in certain settings. Typically, performing a pretest analysis with a complex structure involves either a FE model representing the entire system, or the generation of a modal model with an exhaustive experimental process. The proposed method requires no knowledge of the boundary condition’s dynamic properties, giving it an edge over the use of a pure FE model. This method also has some advantages over experimentally making a modal model, which necessitates the application of a sensor at every relevant output. However, the proposed method only requires one measured output while still estimating the TRF of any other output, offering the versatility of a full model.

6.1.2: Sensor Location Effects

Chapter 5 examined the effects of sensor location error and proposed two possible methods for detecting it in experiments. The first of these methods uses modal contributions to justify the error due to a sensor misplacement. The second uses a sensor location-based model-matching method similar to a FEMU to detect the sensor misplacement. These methods can catch sensor placement error, informing the user if the sensor is not placed as precisely as desired. Each of these methods are experimentally demonstrated in this thesis, with the results indicating the viability of the techniques to detect sensor placement error and aid in experiment design.

The modal contribution approach is validated by performing an experiment with five broadband input signals. The error from applying these signals with a prescribed sensor “error” is justified and understood by examining the input frequency contents with respect to the modal contributions along the range of frequencies and considering how each mode independently varies with a change in sensor location. This also indicates the viability of modal contributions for use in test design and setup, as operators can exercise greater caution for the placement of some sensors depending on the input signals to be applied and the modal contributions of the system.

The model-match approach is validated by performing an experiment to obtain the dynamic response of the beam with three sensor locations and comparing them to an array of models with different sensor locations. In this thesis, multiple metrics for performing the model-match are presented, each of which quantifying the modal similarity of the model and experiment by the relationship of peak frequencies. Of the methods examined, the Total Deviation metric performed the most accurately.

6.2: Future Work

There are many ways to build on what this thesis presents with respect to the technique proposed for estimating the effects of uncertain boundary conditions. Future research involves conducting experiments to better inform the model of the simple structure that will minimize the errors in this experimental technique. This will effectively remove the single largest sources of error observed in this study. Additionally, a parametric study that quantifies the effect of transverse and rotational forces of the stinger in the derivation in relation to the input force could add much value to this work. The quantification of these errors will contribute to further develop the proposed method and increase its significance

to enable higher reliability of the estimation for experimental settings. More advanced research can also investigate the application of this technique to more complex geometries than the cantilever beam used in this thesis, as well as more generalized boundary types.

The use of modal contributions to detect sensor error can benefit greatly from research into the theoretical relationships between the parameters and how they can be objectively quantified and used numerically. Additionally, demonstrations with inputs which have more variable frequency contents could also support this proposed method. Likewise, while the premise of a sensor based model update shows promise, there is more research to do in the future. This research includes the improvement of the technique to achieve more accurate results and detect smaller scale movements. This could be achieved by performing an experiment with the beam with no-contact sensors and using the results to inform a more traditional model update to ensure that the base properties assumed in the creation of the model match those of the physical setup. This method could be further enhanced by an investigation of the extent to which the application of the sensors may alter other material properties of the system, such as the elasticity where the sensor is applied, which this study assumed to be negligible. This research could also be enhanced by the extension of the model into the third dimension, such that the mass of the sensors is no longer on the same axis as the beam, thus enhancing the verisimilitude of the model. Further work also involves research into the application of un-normalized modal contributions to infer sensor location, as touched on in the appendix.

References

- [1] Bedrossian, H., Tinker, M., & Hidalgo, H. (2000). Ground vibration test planning and pre-test analysis for the X-33 vehicle. *41st Structures, Structural Dynamics, and Materials Conference and Exhibit*. Doi: 10.2514/6.2000-1586
- [2] Larson, C., Zimmerman, D., & Marek, E. (1994). A comparative study of metrics for modal pre-test sensor and actuator selection using the JPL/MPI testbed truss. Dynamics Specialists Conference. Doi: 10.2514/6.1994-1689
- [3] Klenke T., Baca, S., et al. “Structural Dynamics Test Simulation and Optimization for Aerospace Components.” *Structural Dynamics Test Simulation and Optimization for Aerospace Components / Meeting Paper Archive*, 22 Aug. 2012, arc.aiaa.org/doi/10.2514/6.1996-3345.
- [4] Mayes, R., Ankers, L., Daborn, P., Moulder, T., & Ind, P. (2019). Optimization of Shaker Locations for Multiple Shaker Environmental Testing. *Experimental Techniques*, 44(3), 283–297. Doi: 10.1007/s40799-019-00347-7
- [5] Rohe, D. P., Nelson, G. D., & Schultz, R. A. (2019). Strategies for Shaker Placement for Impedance-Matched Multi-Axis Testing. *Sensors and Instrumentation, Aircraft/Aerospace, Energy Harvesting & Dynamic Environments Testing, Volume 7 Conference Proceedings of the Society for Experimental Mechanics Series*, 195–212. Doi: 10.1007/978-3-030-12676-6_18
- [6] Vinot, P., Cogan, S., & Cipolla, V. (2005). A robust model-based test planning procedure. *Journal of Sound and Vibration*, 288(3), 571–585. Doi: 10.1016/j.jsv.2005.07.007

- [7] Dahl, Philip R., et al. "Solid Friction Damping of Mechanical Vibrations." AIAA Journal, 17 May 2012, arc.aiaa.org/doi/10.2514/3.61511.
- [8] Smallwood, David O. "Multiple-Input Multiple-Output (MIMO) Linear Systems Extreme Inputs/Outputs." Shock and Vibration, IOS Press, 1 Jan. 2007, content.iospress.com/articles/shock-and-vibration/sav00368.
- [9] "Aerospace Thermal Structures and Materials for a New Era: Progress in Astronautics and Aeronautics." Aerospace Thermal Structures and Materials for a New Era | Progress in Astronautics and Aeronautics, arc.aiaa.org/doi/book/10.2514/4.866364.
- [10] Boubaker, Olfa, and Jean-Pierre Babary. "On SISO and MIMO Variable Structure Control of Non Linear Distributed Parameter Systems: Application to Fixed Bed Reactors." Journal of Process Control, Elsevier, 27 Mar. 2003, www.sciencedirect.com/science/article/pii/S0959152403000040?via=ihub.
- [11] Devine, Timothy A., et al. "Replicating Responses: A Virtual Environmental Test of Unknown Boundary Conditions." SpringerLink, Springer, Cham, 1 Jan. 1970, link.springer.com/chapter/10.1007/978-3-030-12676-6_30.
- [12] Xiao, H., Sheng, M., Liu, Z., & Wei, Z. (2013). The Study on Free Vibration of Elastically Restrained Beams Carrying Various Types of Attachments with Arbitrary Spatial Distributions. *Shock and Vibration*, 20(3), 369–383. Doi: 10.1155/2013/983451
- [13] Irassar, P. V. D., Ficcadenti, G., & Laura, P. (1984). Dynamic analysis of a beam with an intermediate elastic support. *Journal of Sound and Vibration*, 96(3), 381–389. Doi: 10.1016/0022-460x(84)90364-x
- [14] Allen, M. S., Mayes, R. L., & Bergman, E. J. (2010). Experimental modal substructuring to couple and uncouple substructures with flexible fixtures and multi-point

connections. *Journal of Sound and Vibration*, 329(23), 4891–4906. Doi: 10.1016/j.jsv.2010.06.007

[15] Huang, B., Li, Q., Shi, W., & Wu, Z. (2007). Eigenvalues of structures with uncertain elastic boundary restraints. *Applied Acoustics*, 68(3), 350–363. Doi: 10.1016/j.apacoust.2006.01.012

[16] Mignolet, M. P., Soize, C., & Avalos, J. (2013). Nonparametric Stochastic Modeling of Structures with Uncertain Boundary Conditions/Coupling Between Substructures. *AIAA Journal*, 51(6), 1296–1308. Doi: 10.2514/1.j051555

[17] Allen M. S, Mayes R. L. (2007). Comparison of TRF and modal methods for combining experimental and analytical substructures. Proceedings of the 25th International Modal Analysis Conference (IMACXXV), Orlando, FL.

[18] Craig, J. R. (2000). Coupling of substructures for dynamic analyses – An overview. 41st Structures, Structural Dynamics, and Materials Conference and Exhibit. Doi: 10.2514/6.2000-1573

[19] Battiato, G., Fitrone, C., Berruti, T., & Epureanu, B. (2018). Reduction and coupling of substructures via Gram–Schmidt Interface modes. *Computer Methods in Applied Mechanics and Engineering*, 336, 187–212. Doi: 10.1016/j.cma.2018.03.001

[20] Blömeling, F. (2012). Multi-level substructuring combined with model order reduction methods. *Linear Algebra and Its Applications*, 436(10), 3864–3882. Doi: 10.1016/j.laa.2011.02.040

[21] Qiu, J.-B., Williams, F., & Qiu, R.-X. (2003). A new exact substructure method using mixed modes. *Journal of Sound and Vibration*, 266(4), 737–757. Doi: 10.1016/s0022-460x(02)01320-2

- [22] Ismael, G., López-Aenlle, M., Pelayo, F., & Fernández-Canteli, A. (2018). Dynamic Behavior of Supported Structures from Free-Free Modal Tests Using Structural Dynamic Modification. *Shock and Vibration*, 2018, 1–14. Doi: 10.1155/2018/3130292
- [23] Imregun M., Robb D. A., Ewins D. J. (1987). Structural modification coupling dynamic analysis using measured FRF data. Proceedings of the Fifth International Modal Analysis Conference (IMAC V), London, England.
- [24] R. J. Craig, “A Review of Time-Domain and Frequency-Domain Component Mode Synthesis Methods,” *International Journal of Analytical and Experimental Modal Analysis*, Vol. 2, No. 2, 1987, pp. 59-72. - References - Scientific Research Publishing, 2020
- [25] Maia, N. M., & M, M. E. (1998). Theoretical and experimental modal analysis. Baldock, Hertfordshire, England: Research Studies Press.
- [26] Heylen, W., Lammens, S., & Sas, P. (2013). Modal analysis theory and testing. Leuven: Katholieke Univ. Leuven, Departement Werktuigkunde.
- [27] Kundra, T. K. (2000). Structural dynamic modifications via models. *Sadhana*, 25(3), 261-276. doi:10.1007/bf02703544
- [28] Nad, M. (2007). Structural dynamic modification of vibrating systems. *Applied and Computational Mechanics*, 1(1), 203-214.
- [29] Sestieri, Aldo. (2012). Structural dynamic modification. *Sadhana*. 25. 247-259. 10.1007/BF02703543.
- [30] M. Friswell, J. Coote, M. Terrell, S. Adhikari, J. Fonseca, N. Lieven (2005) *Experimental Data for Uncertainty Quantification*.

[31] K. Mendrok, L. Pieczonka T. Uhl (2008) Assessment of uncertainty of experimentally obtained modal parameters.

[32] P. Michaelides, S. Fassois (2008) Stochastic identification of structural dynamics from multiple experiments – experimental variability analysis.

[33] Koruk H. (2017) Quantification and minimization of sensor effects on modal parameters of lightweight structures.

[34] Decker J, Witfeld H (1995) Correction of Transducer-Loading Effects in Experimental Modal Analysis.

[35] Cakar Q., Sanliturk K.Y. (2005) Elimination of transducer mass loading effects from frequency response functions.

[36] Bi S., Ren J., Wang W., Zong G. (2013) Elimination of transducer mass loading effects in shaker modal testing.

[37] Ren J., Wang J., Bi S. (2017) Correction of Transducers Mass Effects from the Measured FRFs in Hammer Impact Testing.

[38] H. Van der Auweraer, B. Peeters, S.Donders (2005) Importance Of Uncertainty In Identifying And Using Modal Models.

[39] Berman A. (1979) Mass matrix correction using an incomplete set of measured modes.

[40] Pcb model 353b03. (n.d.). Retrieved April 05, 2021, from <https://www.pcb.com/products?m=353B03>

[41] PCB model 208C02. (n.d.). Retrieved April 05, 2021, from <https://www.pcb.com/products?model=208c02>

[42] M+P VibPilot measurement hardware. (n.d.). Retrieved April 05, 2021, from <https://www.mpihome.com/en/products/measurement-hardware/mp-vibpilot-measurement-hardware.html>

[43] Lee, D., Ahn, T., & Kim, H. (2018). A metric on the similarity between two frequency response functions. *Journal of Sound and Vibration*, 436, 32-45. doi:10.1016/j.jsv.2018.08.051

[44] Moreu, F., Li, J., Jo, H., Kim, R., Scola, S., Spencer, B., Jr., and LaFave, J. (2015). "Reference-Free Displacements for Condition Assessment of Timber Railroad Bridges." *J. Bridge Eng.*, 10.1061/(ASCE)BE.1943-5592.0000805, 04015052.

Appendix

Modal Contributions and Sensor Output Magnitude

One avenue of research that was pursued was relating the un-normalized Modal Contributions to the change in response when different sensor locations are used. The study performed experiments both in simulations and the real world at 9 frequencies, ranging from 30 to 150 Hz at 15 Hz intervals. At each frequency, the same input load was applied for the three locations of the sensor used previously. The GRMS value indicates the overall magnitude of each response, as given by the equation:

$$GRMS = \sqrt{\frac{1}{N} \sum_{n=1}^N |signal|^2}$$

, where signal is the time domain response of the system at a given location for a given input, and N is the number of discrete points in signal. For these calculations signal is a 10 second steady state window extracted from the original 30 second test or simulation.

Plotting the GRMS value of each signal tip response against the Tip Modal Contributions demonstrates that they are strongly positively correlated. Assuming the centered case for the Modal Contributions then, the change in response magnitude for different sensor locations can be seen in the change in slope. This occurs as the Modal Contribution remains constant at an assumed centered, case, while the GRMS values at each frequency shift to reflect the change in output magnitude due to the change in sensor location.

Ideally, this relationship allows users to observe the potential placement error of a sensor by examining the slope obtained by running a series of sinewave

experiments. This process could help inform the user about sensor location, as well as determine which modes are most responsible for the difference at a given frequency when examining all Modal Contributions and not just their sums. The following figures depict the plots of the log of these values, and the subsequent table compares the slopes for each linear regression line.

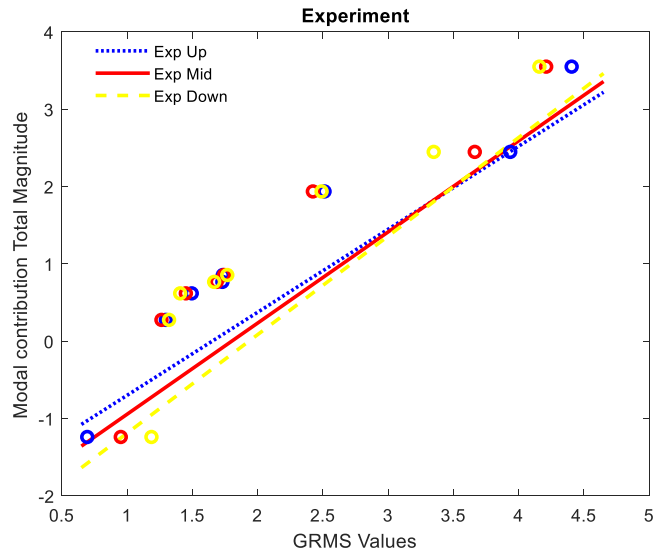


Fig. A-2: Experiment MC Sum vs. GRMS

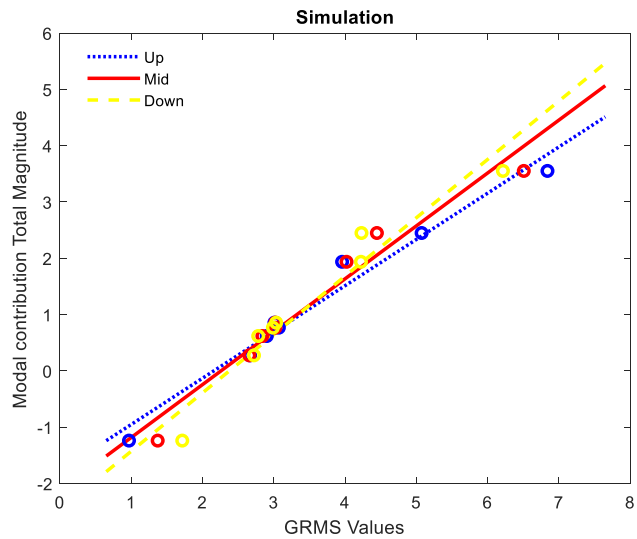


Fig. A-2: Simulation MC Sum vs. GRMS

Table A.1: Linear Regression Slopes

	Up	Centered	Down
Experiment	1.07	1.18	1.27
Simulation	0.82	0.94	1.04

Table A.1 quantifies the change in the slopes, showing how moving the sensor down increases the slope, while moving it up increases it, by roughly equal values. The apparent trend is most evident by the extremes, as the low and high GRMS values are more susceptible to changes due to deviations in sensor location, while the middle values are more muddled and make it more difficult to establish a good trend. The better definition of these middle values and greater precision for the relationships between MC sums and GRMS values comprises some of the on-going work being performed, as well as a deeper understanding of the causes for how the slope changes.